Investigation of Glycosaminoglycans with Ion Mobility-Mass Spectrometry and Gas-Phase IR Spectroscopy

Master Thesis

submitted by

B. Sc. Łukasz Polewski

First Examiner: Prof. Dr. Kevin Pagel

Second Examiner: Prof. Dr. Christoph A. Schalley

Selbständigkeitserklärung

Hiermit bestätige ich, dass die hier vorgelegte Masterarbeit mit dem Titel "Investigation of Glycosaminoglycans with Ion Mobility Mass-Spectrometry and Gas-Phase IR Spectroscopy" nur mit Hilfe der in dieser Arbeit spezifizierten Quellen angefertigt wurde.

Berlin, 20. September 2019

……

Łukasz Polewski

Die hier vorliegende Masterarbeit wurde von März bis September 2019 am Institut für Chemie und Biochemie der Freien Universität Berlin und am Fritz-Haber-Institut der Max-Planck-Gesellschaft unter Anleitung von Prof. Dr. Kevin Pagel durchgeführt.

Danksagung

Zu Beginn dieser Arbeit möchte ich mich bei den Menschen bedanken, die das ganze möglich gemacht haben. Vorne mit dabei Herr Prof. Dr. Kevin Pagel, der mich in seine Arbeitsgruppe aufgenommen hat und mir dieses Thema verliehen hat. Ebenso danke ich Herrn Prof. Dr. Christoph Schalley, der sich bereit gestellt hat diese Arbeit durchzulesen und zu bewerten. Dank gehört auch Herrn Dr. Gert von Helden für die Erlaubnis der Nutzung seiner Geräte.

Auch bin ich der restlichen Arbeitsgruppe Pagel und von Helden zu Dank verpflichtet, da sie mich durch diese Arbeit begleitet haben und immer reichlich Gesprächsstoff und Rat geliefert haben. Besonders zu erwähnen ist hier Christian Manz, der eine Art "Betreuer" für diese Arbeit war und dem zu großen Teilen meine Kaffesucht zu verdanken ist. Auch danke ich Maike Lettow ohne die IR Messungen am imob nur schwer möglich wären. Es war wirklich elektrisierend mit ihr zu arbeiten. Dank gebührt auch dem FEL Team (Eike, Sandy, Wieland) ohne die die IR Messungen nicht mögliche wären. Andreas Zappe ist auch zu erwähnen, der hauptsächlich mit dem Setup der HPLC Anlage an der FU beschäftigt war.

Zu guter Letzt danke ich auch meiner Familie und meinen Freunden für den sozialen und emotionalen Rückhalt während dieser Arbeit und des gesamten Studiums.

Abstract

Glycosaminoglycans (GAGs) are a family of polydisperse polysaccharides, which are widely distributed at cell surfaces and in the extracellular matrix. Although structurally simple at first glance, with a repeating backbone of alternating hexuronic acid and hexosamine dimers, they display a highly complex structure, which results from their heterogeneous sulfation pattern. Even though structurally poorly understood, there has been increasing evidence that GAGs can transchelate gadolinium-based magnetic resonance imaging (MRI) contrast agents. This unintended release of gadolinium is the leading cause of nephrogenic systemic fibrosis. To date, however, the lack of structurally well-defined GAG samples has hindered a detailed elucidation of the underlying mechanism and only soft evidence of a GAG-induced gadolinium release has been reported.

In this work we demonstrate the purification and isolation of GAG fragments from low-molecular-weight-heparin (LMWH) enoxaparin using size-exclusion chromatography. Additionally, we provide the first direct evidence for GAG-gadolinium binding using the synthetic model substance fondaparinux and LMWH enoxaparin. Gas-phase IR spectroscopy and CID-MS/MS experiments revealed possible binding sites of gadolinium on fondaparinux, with surprisingly strong binding contribution from hexuronic acid site chains. This data represent the first direct insights into this complex interaction and will in the future help to unravel the molecular details of GAG-induced gadolinium transchelation from MRI contrast agents.

Contents

List of abbreviations

This list does not contain SI-units and their symbols, signs of mathematical formulas and chemical elements.

ATD	*arrival time distribution*
CCS	*collision cross-section*
CID	*collision induced dissociation*
CRM	*charge residue model*
DT	*drift tube*
Eq.	*equation*
FEL	*free electron laser*
FHI	*Fritz Haber institute*
Fonda	*fondaparinux*
GAG	*glycosaminoglycan*
IEM	*ion evaporation model*
IMS	*ion mobility spectrometry*
IR	*infrared*
IRMPD	*infrared multiple photon dissociation*
IVR	*intramolecular vibrational redistribution*
LMWH	*low molecular weight heparin*
MS	*mass spectrometry*
nESI	*nano electrospray ionization*
SEC	*size exclusion chromatography*
TOF	*time of flight*

1. Introduction

Gadolinium-based imaging probes are used in magnetic resonance imaging (MRI) as contrast agents. As strong chelators they have long been considered as highly stable, inert and safe in clinical setting leaving the body through the kidney in unchanged form.[1, 2] Since the first cases of nephrogenic systemic fibrosis (NSF) have been linked to gadolinium imaging probe injection,[3-5] extensive research has been done to unravel a possible transchelating mechanism.[6] It has been shown that under certain conditions gadolinium is released from its complex *in vivo* when exposed to a competing cation such as Zn^{2+}.[7] Hereby the exchange with linear gadolinium chelators (Gd-DTPA, Gd-DTPA-BMA) showed a higher efficiency compared to macrocyclic chelators (Gd-DOTA).[8] A possible binding partner for the released gadolinium are the glycosaminoglycans (GAGs). GAGs are long, linear and due to their heterogeneous sulfation pattern highly acidic polysaccharides.[9] They consist of disaccharide subunits and form chains with a length of up to ~100 disaccharides. As major component of the extracellular matrix in human tissue they can be found in every part of the human body. They mainly play a role in various physiological processes such as tissue shock absorption, lubrication, supporting collagen and elastin keeping the protein fiber in balance.[10] As highly anionic species they possess a high metal binding affinity. Nuclear magnetic resonance experiments showed that in presence of zinc and GAGs an increase of the measured T1-relaxivity was observed.[11] This indicates a possible transchelation of gadolinium from the complex agent to the GAG. Experiments in solution can only provide limited evidence due to the high complexity of the samples. The near clean room environment of the gas phase allows isolation and investigation of specific species even in a complex mixture. Therefore in this work gas phase techniques such as mass spectrometry (MS), ion mobility spectrometry (IMS) and infrared (IR) spectroscopy were used to provide further insight into the possible binding of gadolinium to GAGs and its binding sites.

2. Theory

2.1 Glycosaminoglycans

Glycosaminoglycans are linear and highly acidic polysaccharides. They are ubiquitous molecules, which exhibit a wide range of biological functions and are involved in the tissue integrity, cell recognition, migration, proliferation and protein folding.[10] Although structurally simple at first glance, with a repeating backbone of alternating hexuronic acid and hexosamine dimers, they display a highly complex structure, which results from their heterogeneous sulfation pattern. GAGs are classified into several different groups depending on their backbone composition, possible sulfation sites, connectivity and average polysaccharide size (see figure 1). The simplest GAG is hyaluronic acid, which is known for its wide application in cosmetics. It consist of repeating units of D-glucuronic acid and *N*-acetyl-glucosamine, which are alternating β-1,4 and β-1,3 linked.[12] Since hyaluronic acid is not sulfated the only variable is the size of the observed polysaccharide. Keratan sulfate differs from the other GAGs due to the missing hexuronic acid which is instead replaced by a galactose. The galactose is β-1,4 linked to a *N*-acetyl-glucosamine, which is then β-1,3 linked to the next disaccharide subunit. Keratan sulfate possesses two possible sulfation sites at the *6-O* position at the galactose unit and the *6-O* position at the *N*-acetyl-glucosamine.[13] Chondroitin sulfate consists of D-glucuronic acid, which is β-1,4 linked to *N*-acetyl-glucosamine. The disaccharide units are β-1,3 linked to each other. Possible sulfation sites are the *2-O* position of the glucuronic acid and the *4-O* and *6-O* position of the *N*-acetyl-glucosamine.[14] Dermatan sulfate is very similar to chondroitin sulfate, with the only difference being an L-iduronic acid instead of the D-glucuronic acid in the disaccharide.[14] The most complex GAGs are heparin and heparan sulfate. They consist of either an iduronic or a glucuronic acid, which is β-1,4 linked to a glucosamine. The disaccharide units are α-1,3 linked to each other. Again there are three possible

sulfation sites, the *2-O* position at the hexuronic acid, the *2-N* position at the glucosamine and the *6-O* position at the glucosamine. Additionally the *N*-position can be either acetylated or protonated.[15)]

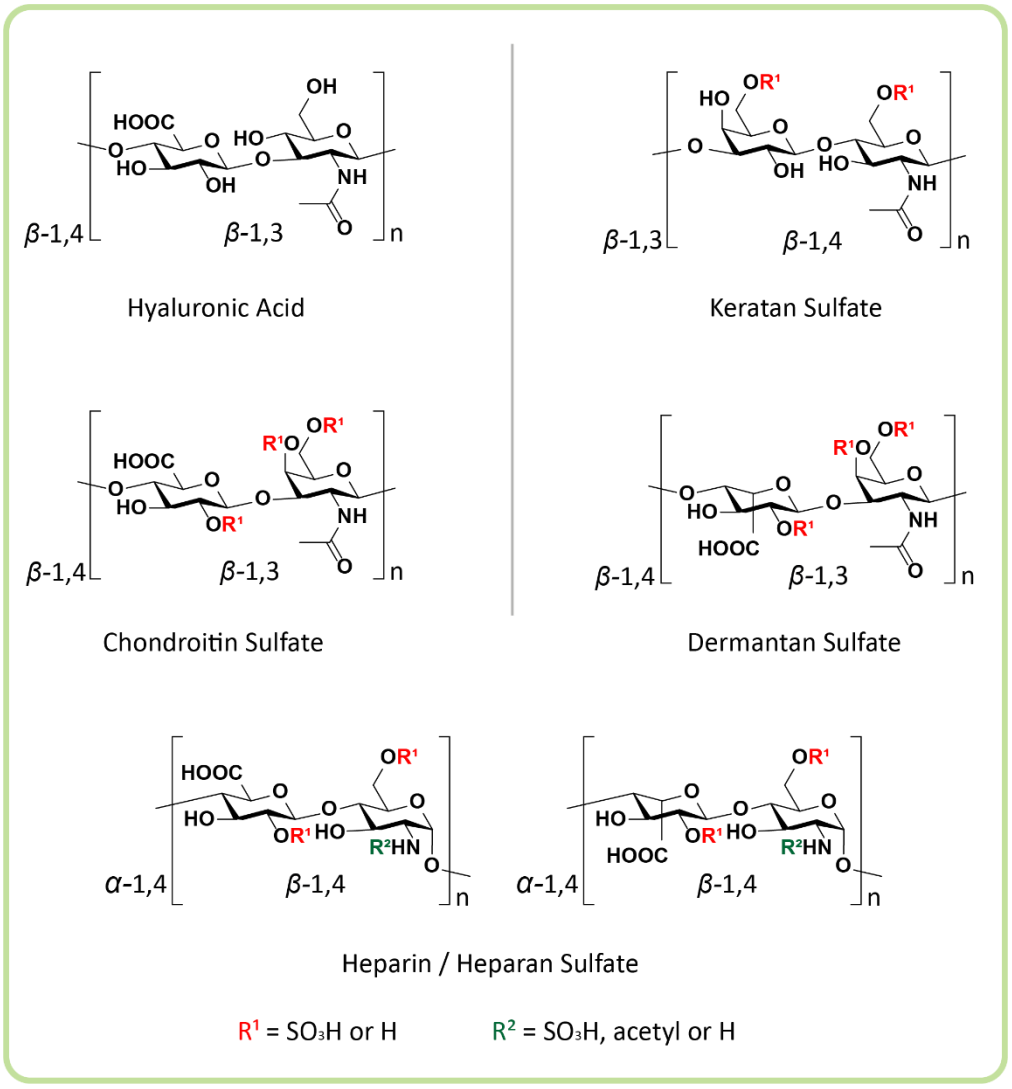

Figure 1: *Several different groups of GAGs classified due to their disaccharide backbone and sulfation sites.*

A very rare modification of heparin and heparan sulfate is the sulfation on the 3-*O* position of the hexuronic acid. The difference between heparin and heparan sulfate is the proportion of the two different hexuronic acids. Heparin consists mainly but not

exclusively of L-iduronic acid while heparan sulfate mainly consists of D-glucuronic acid.[15] For an easier structural elucidation or to enhance medical potency and reduce risk factors these GAGs can be cleaved chemically[16] or enzymatically.[17] Depending on the used procedure different fraction are obtained, which differ in their average polysaccharide length. Most often the non-reducing terminal hexuronic acid eliminates on the 4-5-C position to form a double bond.[15] An advantage of this double bond is the easy detectability through UV-spectroscopy due to an absorption band at 232 nm.[18] The most notable cleaved GAGs are the low molecular weight heparins (LMWH) (see figure 2) with wide use as a substitute medicine for unfractionated heparin due to their lower risk factors.[19]

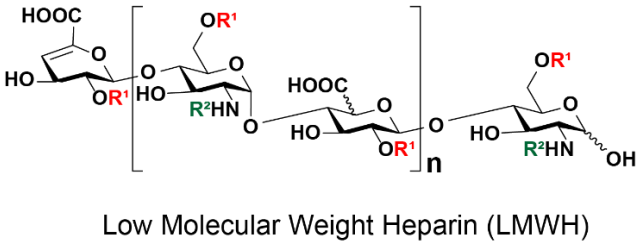

Figure 2: *Generic molecular formula of fractionated heparin (low molecular weight heparin). The site specific functionalization remains the same.*

Average fraction sizes range between 3 kDa (Bamiparin) to 7 kDa (Tinzaparin) while unfractionated heparin possesses an average weight of 25 kDa.[20]

2.2 Glycan Analytics

The classical challenges of *N*- and *O*-glycan analysis are emerging out of three different molecular properties (see figure 3): composition, connectivity and configuration. Composition describes the monosaccharides and their sequence inside the glycan. Connectivity is the regiochemistry of the bonds between the monosaccharides, which are most often 1-3, 1-4 or 1-6 linked and also possible branches in the structure. The configuration describes the stereochemistry of the glyosidic bond at the anomeric center.[21)]

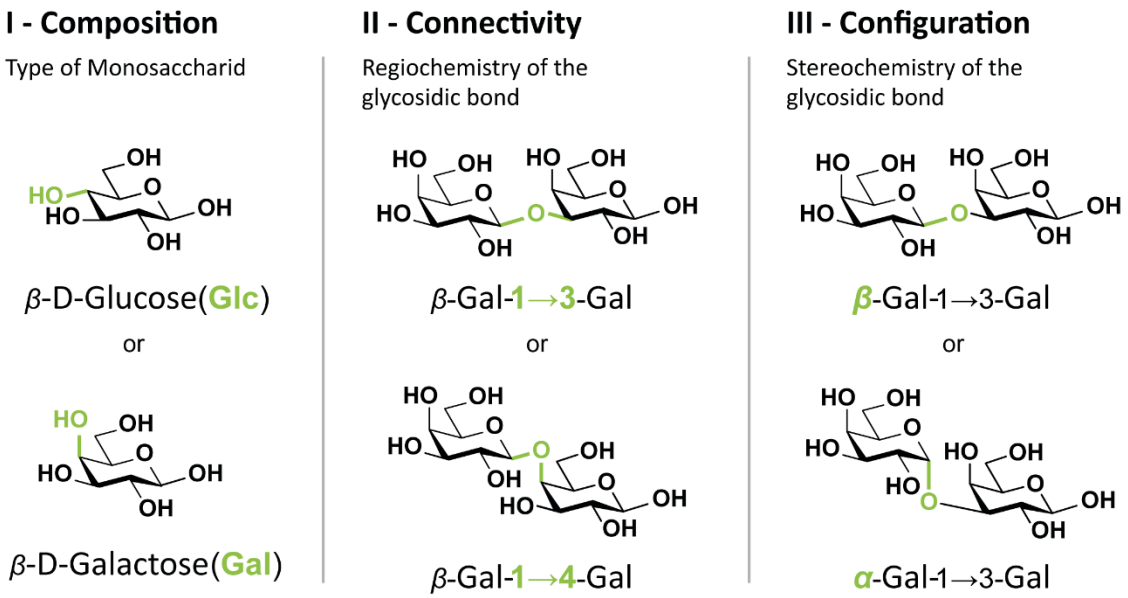

Figure 3: *Structural properties of glycans.*

Most of these analytical challenges play no role in GAG analytics since all of the GAGs consist of a repeating backbone with the same linkage and stereochemistry between the repeating disaccharide subunits (see figure 4). Only for heparin, heparan sulfate and the corresponding low molecular weight fraction the problem of the composition holds. For the hexuronic acid either an iduronic acid or a glucuronic acid can be incorporated. These both acids are C5-epimers and therefore impossible to be distinguished by their *m*/*z*-ratio

alone. Classical techniques such as NMR spectroscopy can distinguish epimers from each other[22] but the high sample amount requirement hinders the use. It was shown that electron detachment dissociation (EDD) is able to produce C5-epimer specific fragments in heparin sulfate tetrasaccharides, which could help in the identification of unknown samples.[23, 24] Additionally ion mobility spectrometry (IMS) is capable of distinguishing the C5-epimers in up to hexasaccharides.[25] The major challenge in GAG analysis, which all GAG types except hyaluronic acid share, is the determination of the sulfation pattern. For small polysaccharides up to dodecamers standard fragmentation techniques like electron transfer dissociation (ETD)[26] and collision induced dissociation (CID) in combination with previous derivatization have shown great capability.[27] Larger sequences of GAGs are yet to be analyzed.

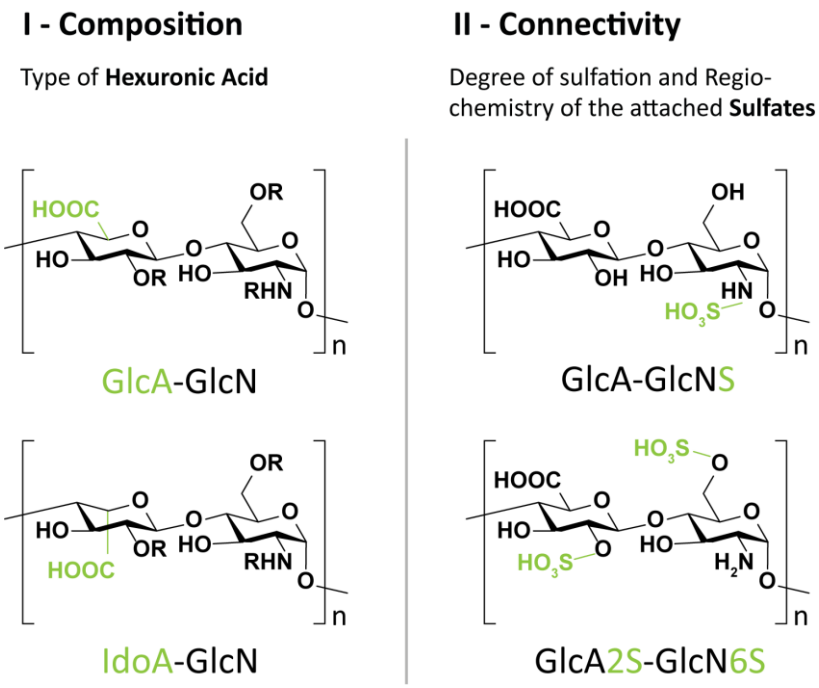

Figure 4: *Structural properties of GAGs, in particular heparin and heparan sulfate.*

2.3 Glycosaminoglycan-Metal Binding

GAGs as highly anionic species are prone to cation binding. While monovalent cations seem to prefer sulfate groups as coordination sites due to their higher acidity divalent ions, in particular calcium, possess a high dependence on the carboxylic acid group of the hexuronic acid subunits.[28] NMR titration experiments showed a higher acidity of iduronic acid in presence of calcium while the effect on the C5-epimer glucuronic acid seemed only meagre.[29] The presence of a metal ion induces rapid conformation changes in GAGs depending on the used cation.[30-32] These changes not only deform the polysaccharide into a more compact form but also induce conformational changes in the monosaccharides. Iduronic acid in heparin is equilibrated between a chair conformer ($^1C_4$) and a skew-boat form ($^2S_0$) (see figure 5).[33] The presence of metal ions favors the formation of the chair conformer.[31]

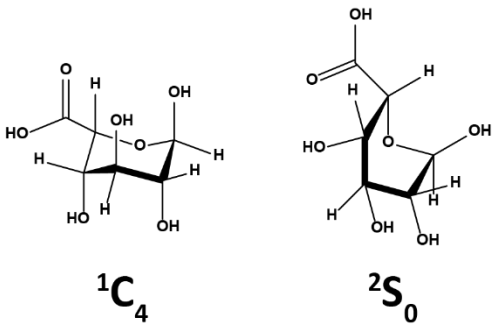

Figure 5: *Iduronic acid in its two most favorable conformers: the chair ($^1C_4$) and the skew-boat form ($^2S_0$).*

The effect of trivalent cations on GAGs is largely unknown. NMR studies have shown that the triply charged lanthanum cation behaves similarly to calcium, binding favorably on specific sites near the hexuronic acids with a higher binding affinity.[34] It is expected that gadolinium for instance, which possesses a similar ionic radius as calcium, will also behave similar to its divalent equivalent.

3. Methods

3.1 Size-Exclusion Chromatography

A technique to separate mixtures of analytes by their hydrodynamic radius is the size exclusion chromatography (SEC). Hereby a column is filled with porous beads with a variable cavity size and the analyte is led through it. Compared to other chromatographic methods the separation is not based on intermolecular interaction of the analyte with the functionalized bead surface (hydrogen bridges, electrostatic interaction) but instead solely on the capability of entering the bead pores (see figure 6). Smaller analytes fit into more bead pores than larger ones. When they are inside of a pore the analyte cannot be dragged along with the mobile phase. This results in a separation of the injected mixture according to their size. As mobile phase most often water is used which is eluted isocratically. This separation works especially well for polymers where each polymer length is assignable to a peak in the chromatogram.[35)]

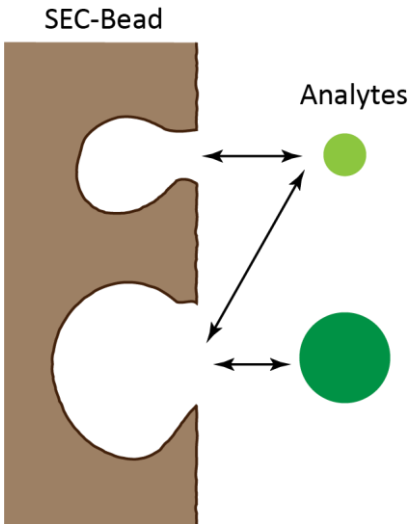

Figure 6: *Illustration of a SEC separation. Smaller analytes can enter more pores and therefore elute later.*

3.2 ESI/n-ESI

The electrospray ionization (ESI) is a very soft ionization technique which was first used in 1968 by Malcolm Dole. It is based on the effect of the electrospray where a liquid ejects out of an electrically charged needle and moves toward an oppositely charged plate. When leaving the needle, through a so-called Taylor cone which forms due to the voltage gradient between needle and plate and the surface tension of the liquid, the liquid forms small droplets which further shrink the further they travel.[36] When the liquid evaporates completely only the charged molecules remain. There are two major mechanisms involved in the formation of the single ions, the Ion Evaporation Model (IEM) and the Charge Residue Model (CRM).[36] Both of these mechanisms emerge out of the same property, the increasing charge density on the surface of the liquid droplets. When the charged droplets leave the needle and the solvent evaporates the charge stays in the droplet. After the maximum charge density, the so called Rayleigh limit, is achieved the charge density on the surface of the droplet is reduced. In the ion evaporation model the droplet undergoes evaporation until a point where the analyte gets ejected by the electric field emitted by the droplet at the Rayleigh limit,[36] leaving the droplet with less charge to evaporate further and eject another ion into the gas phase (see figure 7). In the CRM the droplet gets smaller until a point at which the coulomb forces at the surface are so strong that the droplet undergoes a coulomb explosion. After the explosion the analyte is now dispersed in many smaller droplets with a lower surface charge density. These smaller droplets repeat the evaporation and coulomb explosion steps until only the charged analytes remain. Small ions tend to be released by the IEM, while larger ions are often formed by the CRM. Molecules ionized by ESI often carry multiple charges

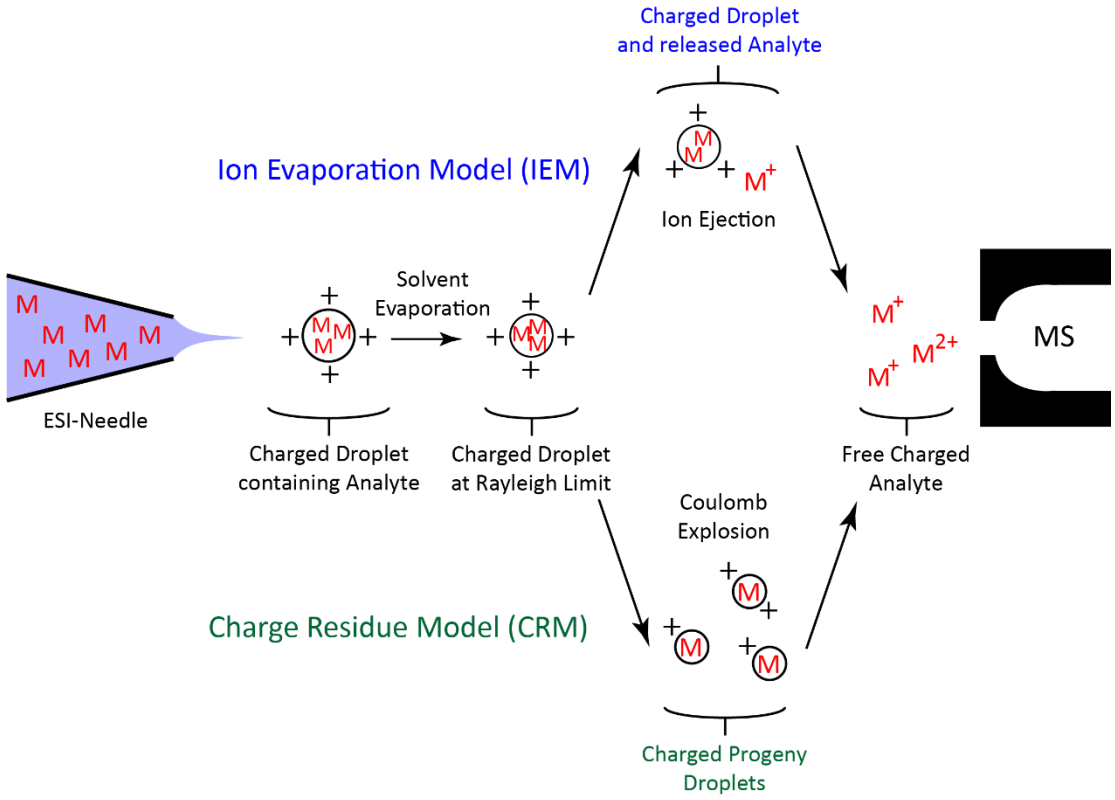

Figure 7: *Schematic illustration of the different models for ESI: IEM and CRM.*

depending on the ionized molecule, in contrast to similar soft methods like matrix assisted laser desorption/ionization (MALDI), which predominantly generates singly charged ions. This technique can be used to form either positively as well as negatively charged ions. Because of the softness of this method, it is widely applied in all fields of biochemistry analysis[37] like proteomics, glycomics and lipidomics. A variation of ESI is nano-ESI (n-ESI). In n-ESI a much smaller needle with a reduced diameter is used. This reduces the amount of needed sample drastically to achieve a lasting ion current.[38]

3.3 Ion Mobility Spectrometry

The separation capability of mass spectrometry is limited to only the mass-to-charge-ratio. For cases with different mass it is enough to distinguish separate species but when it comes to structural similar isomers this technique often fails. Additional separation of isomers prior to the *m*/*z* detection can help to solve this problem. There are several widespread methods that are used, most commonly high performance liquid chromatography (HPLC) and gas chromatography (GC). Both of these methods require often multiple minutes to be performed and therefore are limiting the sample throughput. An emerging technique in this field is ion mobility spectrometry (IMS) in which the ions are drifting through a gas-filled tube (see figure 8).[39]

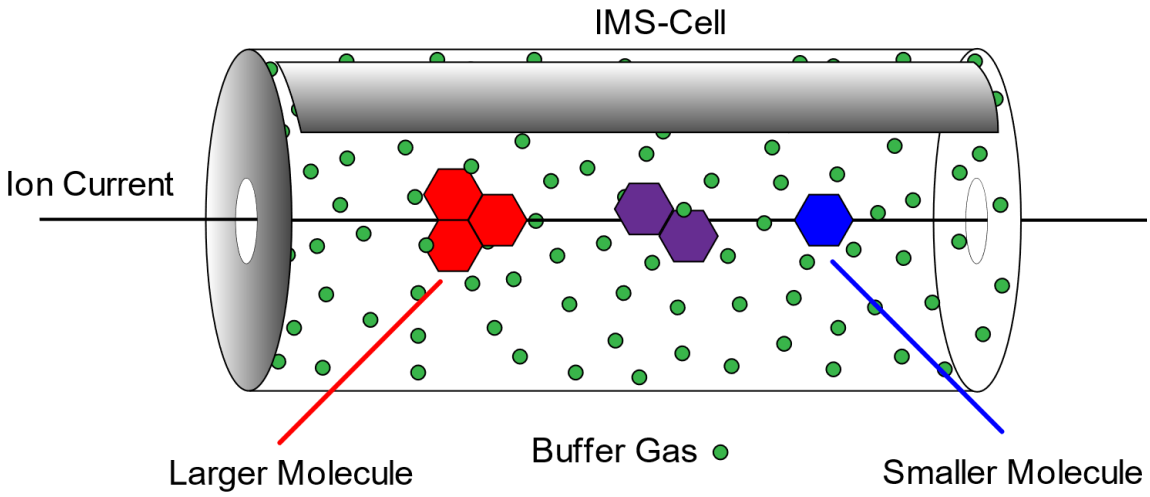

Figure 8: *Illustration of an IMS cell.*

The ions are guided by an electric field and the collision between the ions and the neutral buffer gas slows them down.[39] Larger ions collide more frequently with the buffer gas than smaller ions and therefore need a longer time to traverse through the drift cell. Also

higher charged ions experience a stronger pulling force through the electric field *E*, which increases their velocity. Analogous to retention times in HPLC, drift times are dependent on various instrumental parameters. A device independent quantity to describe the drifting behavior is the collision cross-section (CCS). It is derived from the ion mobility *K*, which is linked to the experimental value t_d (drift time) and l (length of drift tube)(see equation 1).[39]

$$K = \frac{v_d}{E} = \frac{l}{t_d \cdot E} \tag{1}$$

When normalized to standard conditions with T_0 = 273 K and p_0 = 1013 mbar the reduced ion mobility K_0 is obtained (eq. 2).[39]

$$K_0 = K \cdot \frac{T_0}{T} \cdot \frac{p}{p_0} \tag{2}$$

The CCS-value Ω can then be deduced by the Mason-Schamp equation (eq 3.) shown below.

$$\Omega = \frac{3}{16}\sqrt{\frac{2\pi}{\mu \cdot k_B \cdot T}} \cdot \frac{ze}{N \cdot K_0} \tag{3}$$

The variables *ze* describes the charge of the ion, μ the reduced mass of the ion-gas pair and k_B the Boltzmann constant. Even though the CCS-value is often described as completely

device independent this only holds when certain conditions are met. The measurements must be performed under low-field-condition.[39] This means that the electric field is low compared to the buffer gas density (see eq. 4).

$$\frac{E}{N} < 10^{-20}\ V \cdot m^2 \tag{4}$$

The problem arises from the reduced ion mobility K_0. Only when E/N is low enough the ion mobility is nearly independent from it. This behavior is at the moment only empirically described seen in equation 5 below. The alpha-values α_x are empirical scaling values which describe the impacted of the field dependence.

$$K_0\left(\frac{E}{N}\right) = K_0(0)[1 + \alpha_2\left(\frac{E}{N}\right)^2 + \alpha_4\left(\frac{E}{N}\right)^4 + \ldots] \tag{5}$$

The most commonly used methods to measure IMS arrival time distributions (ATDs) and CCS-values are the drift tube ion mobility spectrometry (DTIMS) and the traveling wave ion mobility spectrometry (TWIMS). The difference consists in the form of the applied electric field. In DTIMS a homogenous linear electric field is applied from one end of the IMS-cell to the other. TWIMS uses a wave formed electric field[40] (see figure 9), which is pushing the ion with a wave-like frequency where bigger ions can roll over depending on the size and velocity of the wave. Smaller ions are being dragged by the wave longer than larger ones, this further increases the separation capability of a TWIMS instrument compared to DTIMS.[39]

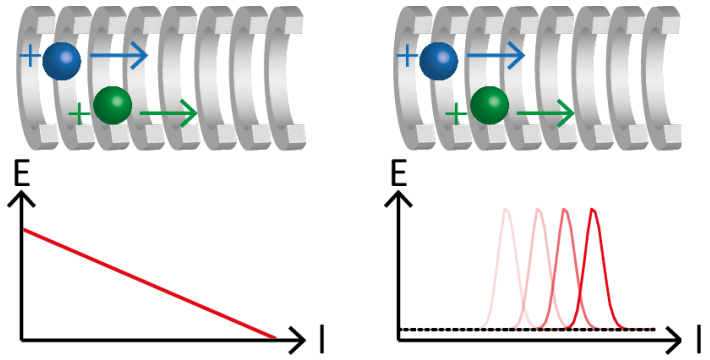

Figure 9: *Comparison of the electric field of DTIMS (left) and TWIMS (right).*

A major disadvantage of TWIMS is that the electric field cannot be fully mathematically described and often exceeds the low-field-limit extensively. This means that the ion mobility *K* cannot be directly calculated out of the ATDs. Therefore a calibration procedure is required to acquire CCS-Values out of a TWIMS instrument. Additionally the indirectly measured CCS-values have an increased error margin compared to a DTIMS obtained value.

3.4 Collison-Induced Dissociation

One of the most common methods for ion activation/fragmentation is collision-induced dissociation (CID). In this method the fragmentation is reached by a collision between the analyte and an inert gas (most often argon or nitrogen). After several inelastic collisions between the charged analyte and the neutral gas, the analyte fragments.[41] The process behind the dissociation can be explained as a transformation of kinetic energy into internal energy which then leads to subsequent decomposition of the ion. Since the collisions between buffer gas and ion are not completely inelastic the total available kinetic energy is not equal to the internal energy resulting from a collision.[41] The conversion rate of the kinetic energy (E_{kin}) into internal energy (E_{int}) depends on the mass of the ion (m_p) and on the mass of the used buffer gas (N) (see equation 6)

$$E_{int} = \left(\frac{N}{m_p+N}\right)E_{kin} \qquad (6)$$

Therefore heavier molecules require more collisions to reach the same internal energy as lighter ones. The fragmentation following a collision induced excitation can be described as a unimolecular dissociation where the internal energy is distributed into different vibrational modes which results, similarly to infrared multiple photon dissociation (IRMPD), into the favorable fragmentation at the weakest bond.[41]

3.5 Infrared Multiple Photon Dissociation based Action Spectroscopy

The commonly known absorption spectroscopy measures the difference between the light intensity before and after the interaction with the analyte. This approach works great when the analyte concentration is high compared to the light intensity. This is most often the case for solid state or liquid analysis. In gas-phase spectroscopy the concentration of analytes is too low to measure a difference in the light intensities.[42] Especially the density of ion-based gas-phase spectroscopy is limited by the space charge limit. Therefore instead the light intensity is increased dramatically to a point where the high light intensity is inducing physical changes such as dissociation processes or conformational changes in the analyte (the so-called action spectroscopy). By plotting the fragmentation yield against the wavenumber an "absorption-like" spectrum can be recorded.[42]

IRMPD uses low energy photons from the infrared region ($\lambda \sim 700 - 1000$ nm), which excite vibrational modes. Since the energy of a single infrared photon is often not enough to stimulate a dissociation, action spectroscopy with low energy photons requires multiple photons to be absorbed.[43] These photon absorptions happen in quick succession but nevertheless the fragmentation site is independent from the wavenumber and stimulation point. Most often the weakest bond in the molecule breaks. This is due to the much faster intramolecular vibrational redistribution (IVR) process. IVR depopulates the excited vibrational state into the vibrational background states in the molecule before a second photon can be absorbed.[28] The short vibrational lifetime caused by IVR broadens the observed absorption lines. Additionally the anharmonicity of the populated vibrational modes leads to an internal energy dependent red-shift of the observed absorptions.[42] Therefore spectra obtained from more easily fragmented ions show a closer resemblance to theoretically calculated (linear) spectra.

4. Aim

The transchelation of gadolinium from MRI contrast agents poses a huge threat for the health of patients worldwide. The understanding of the underlying process and the effects of an increased gadolinium content in tissue is still under investigation and could lead to a reevaluation of the approved MRI contrast agents. The aim of this work is to obtain direct evidence of a gadolinium-GAG binding and investigate the possible binding sites with a combination of different gas phase techniques such as MS, IMS and IRMPD spectroscopy.

5. Results

5.1 MS Measurements on Enoxaparin

As suitable substance to investigate the Gd-GAG binding the LMWH enoxaparin was chosen. Heparin and its fraction show the highest degree of possible sulfation and are therefore more prone to show results in regard of the gadolinium binding. Since the whole heparin is too large, heavy and heterogeneous with an average mass of about 25 kDa it cannot be investigated by standard gas phase techniques. The LMWH enoxaparin on the other hand possesses an average mass of ~4.5 kDa, which makes it suitable to be analyzed by mass spectrometry even for a very heterogeneous mixture. Enoxaparin is commercially available as a sodium salt. Therefore a measurements in the ion negative mode is preferred. The first measurements of enoxaparin-sodium (Enox-Na) showed a very broad spectrum with no defined species. This is due to extensive cluster formation induced by the high sodium content (see figure 10).[44] Therefore the enoxaparin was desalted to obtain

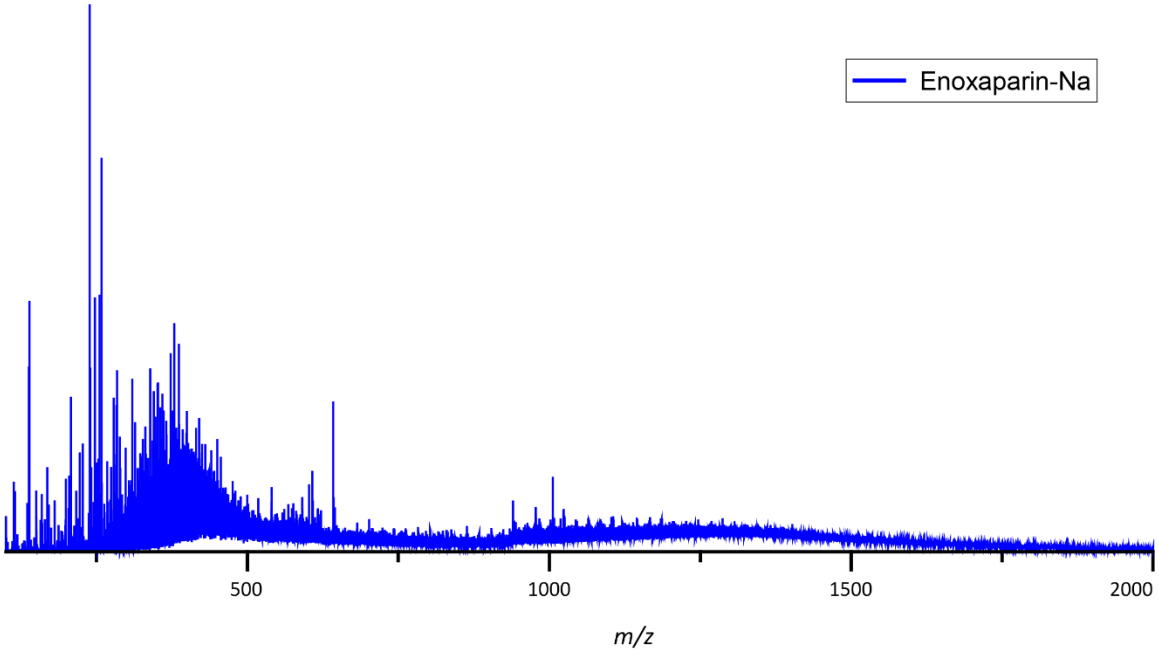

Figure 10: *Mass spectrum of enoxaparin-sodium showing very little clear signals.*

a comparably sodium-free sample. The now desalted enoxaparin showed more clear peaks with noticeable isotope pattern in its spectrum (see figure 11). Especially, but not only, the *m*/*z* region between 400 and 600 shows many assignable mass peaks (see figure 12).

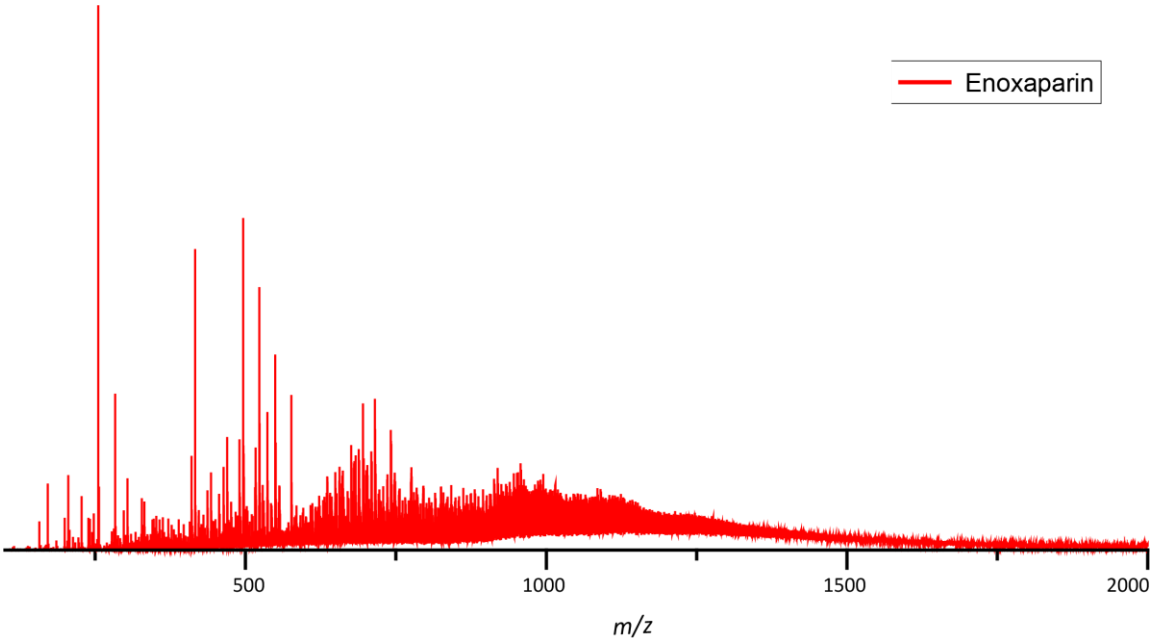

Figure 11: *Mass spectrum of enoxaparin after desalting shows more clear signals.*

In this region many species are visible where the observed charge state (*z*) equals the number of disaccharide units (*N*) (see figure 12). The peaks are assigned with the *N*/*z* annotation. All species are completely protonated with no salts attached to them. The largest observed species corresponds to the *m*/*z* 576. This is the fully sulfated species where out of three possible sulfation sites (*S*) per disaccharide unit all are occupied (for $N = 1$, $S = 3$; for $N = 2$, $S = 6$ etc.). Since the disaccharides are linked through glyosidic bonds to one another one would expect a mass difference between for example $N/z = 2/2$ and $N/z = 3/3$ but due to the additional condensation on the terminal hexuronic acid group this difference vanishes and the species become only distinguishable by their respective isotope pattern ($\Delta m/z = 0.5$ for $z = 2$ and $\Delta m/z = 0.33$ for $z = 3$ etc.).

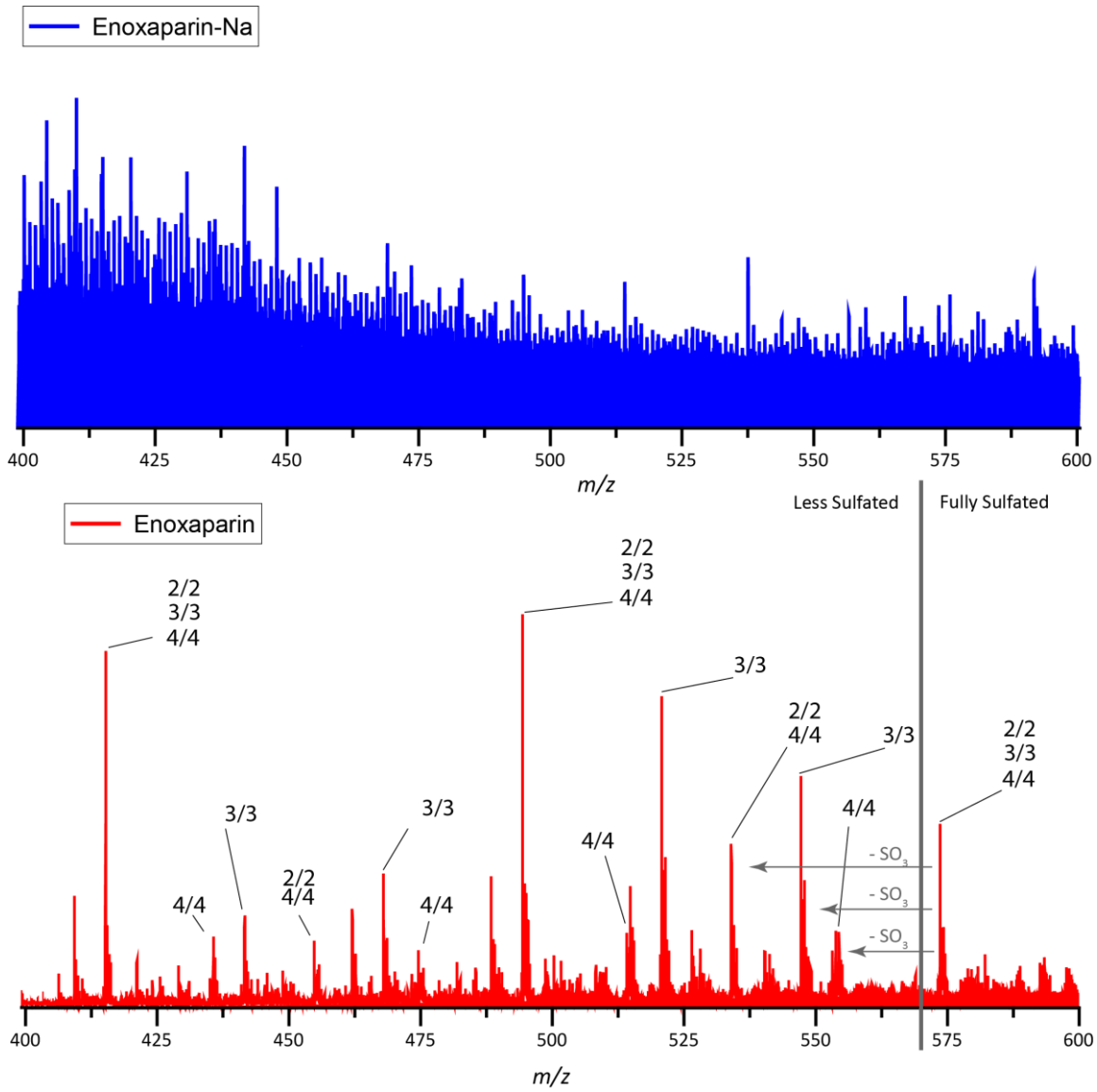

Figure 12: *Zoom on the mas range from m/z 400-600 shows many assignable peaks for the desalted enoxaparin.*

Noticeable is that the lowest observed species in this mass range is *m/z* 416. This mass equals a tetrasaccharide (*N* = 2) with two sulfates attached, to a hexasaccharide (*N* = 3) with three sulfates attached to it and an octasaccharide (*N* = 4) with four sulfates attached to it.

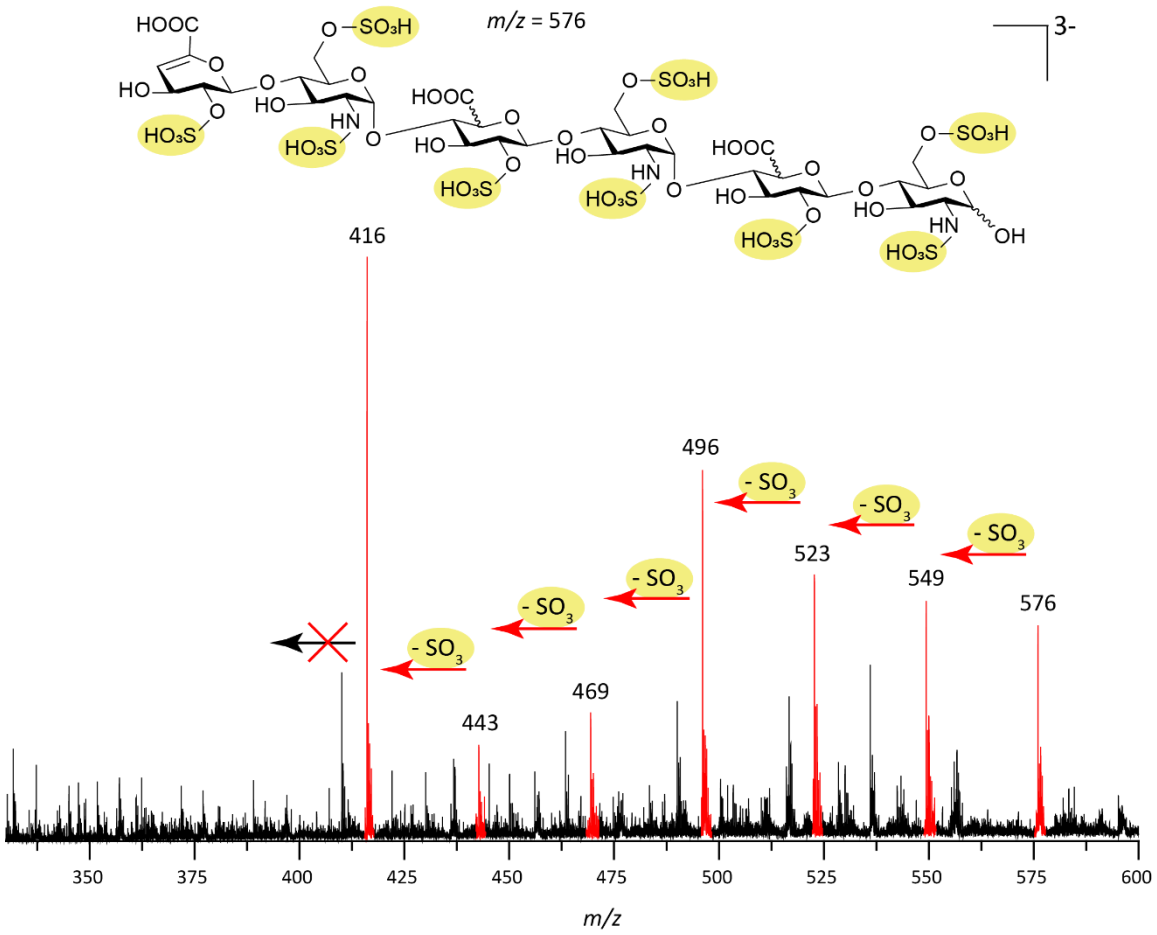

Figure 13: *The desulfation pattern of the fully sulfated 3/3 enoxaparin (m/z 576). Desulfation only occurs till a point where the number of sulfates equals the charge state.*

CID fragmentation of the observed species was performed. Since GAGs are very prone to sulfate loss when energy is applied, the desulfation pattern is dominating the fragmentation products (see figure 13). Desulfation always happens by loss of a neutral SO_3 unit. This means when a proton is attached to the sulfate the proton is transferred to the hydroxy group resulting from the desulfation. The CID measurements of several different species and charge states showed that the minimal number of sulfates attached to the enoxaparin molecular ion always equals the charge state. This is a very good indicator that all the charges introduced through the ESI process sit on the sulfates and not on the carboxylic acids, which could also hold a negative charge. This observation also

matches the chemical intuition since sulfates are, under normal conditions, more acidic than carboxylic acid groups. Additionally the CID experiments showed that sulfate groups that hold a negative charge will not fragment with the known neutral loss mechanism and even at higher energies will remain on the enoxaparin.

5.2 Enoxaparin-Gadolinium Binding

To the desalted enoxaparin sample gadolinium nitrate was added ($Gd(NO_3)_3$). The broad isotope pattern of gadolinium (*M* = 154-160 g/mol) complicates the search for a possible cross peak with enoxaparin since the intensities of the measured species will be distributed across a wide mass range. At the same time the very unique isotope pattern of gadolinium makes the assignment of possible peaks straightforward. For the enoxaparin two peaks that correspond to a gadolinium based species were found. The peaks at *m*/*z* 628 and 601.3 match the *m*/*z* of the triply charged hexasaccharides. Both species are highly sulfated with

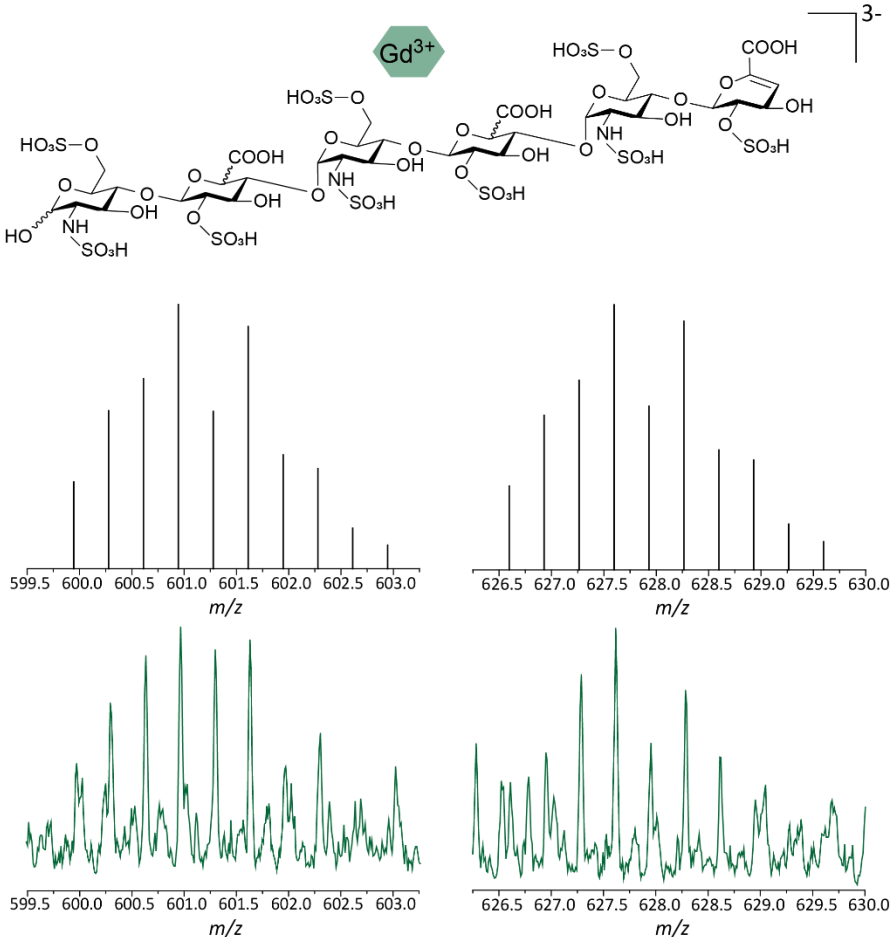

Figure 14: *The measured species (bottom) match the calculated masses and isotope patterns (top) of the hexasaccharide (8 and 9 sulfate groups) with a gadolinium attached to it.*

the one at *m/z* 628 possessing nine out of nine possible sulfations and the one at *m/z* 601.3 with one sulfation less. The measured isotope pattern matches the theoretically calculated ones largely (see figure 14) to some degree of deviations.

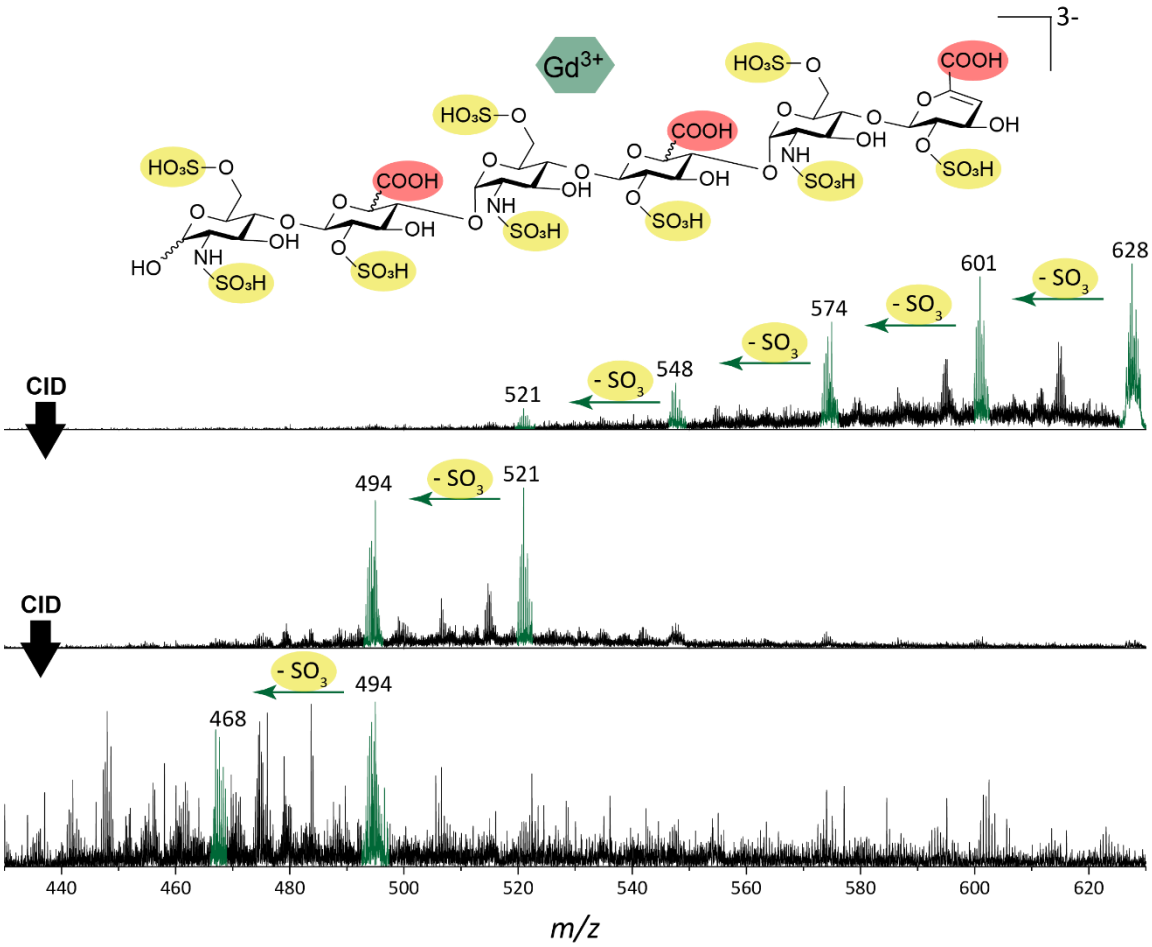

Figure 15: *The desulfation pattern of the fully sulfated 3/3 enoxaparin-gadolinium species (m/z 628). As before desulfation only occurs till a point where the number of sulfates equals the charge state.*

This slight deviation is due to overlaying "background" signals resulting from the very heterogenous enoxaparin mixture. The enoxaparin-gadolinium species was isolated and CID experiments were performed on them. The experiments showed similar results to the

ones without a gadolinium attached to enoxaparin. Again we see mainly the desulfation with some minor fragment channels likely resulting from impurities in the same mass range. A triply negatively charged species with a gadolinium attached to it has six negative charges sitting on it to compensate the three positive charges from the gadolinium. We see that in the case of the deprotonated enoxaparin all charges sit on the sulfate groups preventing them to fragment off under neutral loss. If the same conditions apply to the gadolinium species six charges would sit on the sulfate groups, which in the case of the fully sulfated hexasaccharide would mean that out of the nine sulfate groups three would fragment off. Instead we still see six sulfate losses (see figure 15). This implies that the additional charges introduced due to the gadolinium are not sitting at the more acidic sulfate groups but instead on the carboxylic acids. This matches the expected results since calcium, which possess a very similar ionic radius, shows the same behavior binding mainly on the carboxylic acid functions.[34)]

5.3 Size-Exclusion Chromatography on Enoxaparin

To investigate the enoxaparin-gadolinium binding further a less heterogenous sample is needed. One of the major limiting factors is the overlap of the $N = z$ species, especially since these species are the most present ones in the mass spectrum. The most effective way to separate them is by SEC due to its capability to separate solely on the basis of size.

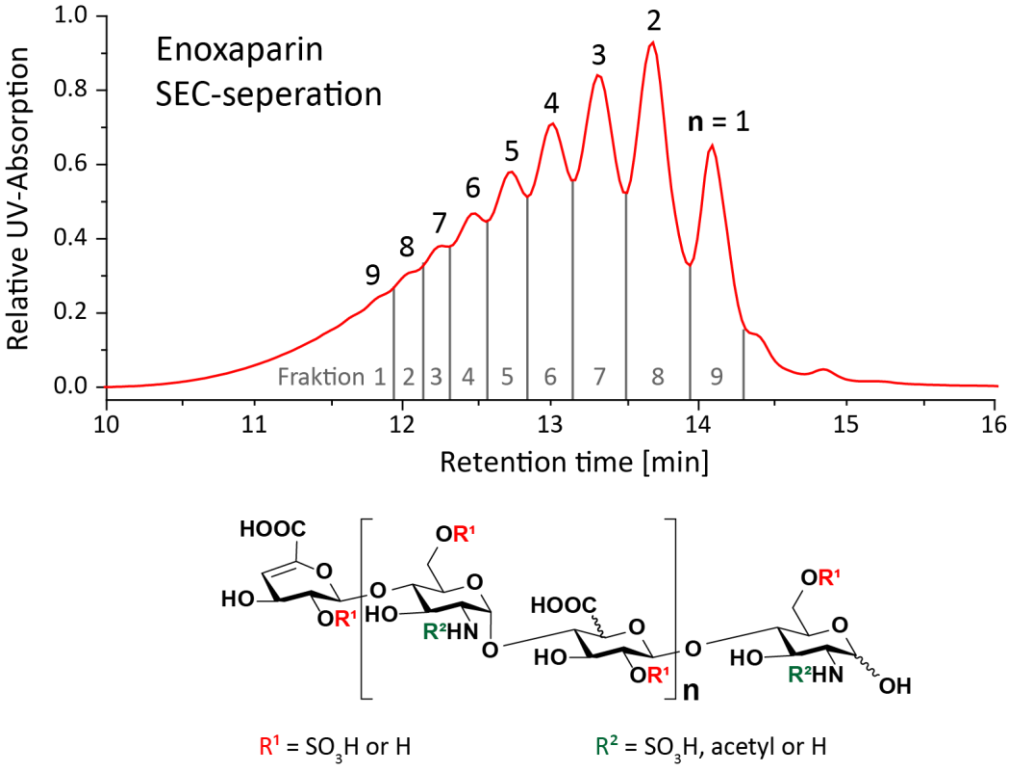

Figure 16: *The SEC chromatogram of enoxaparin. Nine different fractions were obtained.*

Additionally SEC desalts the sample, which is necessary to further analyze the sample. The fractions were detected with a UV-absorption detector at 232 nm wavelength. Nine fractions were obtained and analyzed by mass spectrometry. The fraction number 9 showed the best results with only minor amount of impurities. Fraction nine corresponds to the tetrasaccharide, fraction eight to the hexasaccharide, fraction seven to the

octasaccharide etc. (see figure 16). Fractions 7-9 showed promising results. The separation of earlier fractions was too small to work further with them.

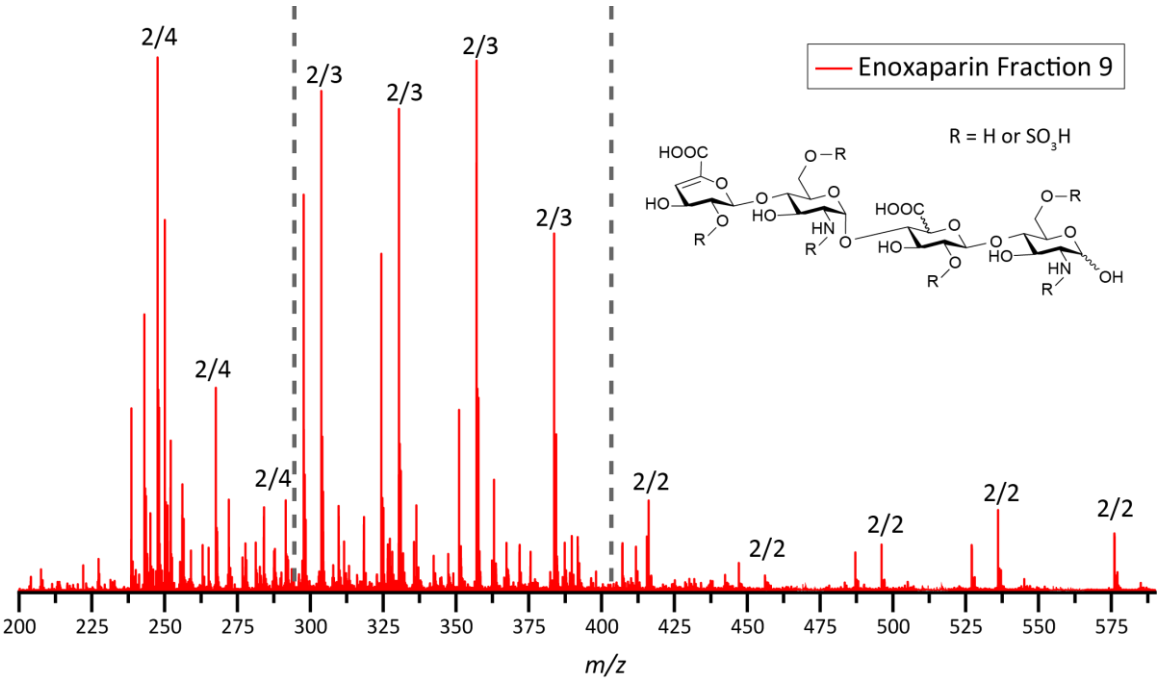

Figure 17: *Mass spectrum of SEC separated enoxaparin tetrasaccharides corresponding to the fraction nine.*

The mass spectra showed that in contrast to the mixture, the size separated GAGs preferably ionize to the charge state $z = N+1$ (see figure 17).

5.4 Enoxaparin Stability Measurements

To investigate the effect of gadolinium on the desulfation behavior more firmly energy resolved MS was performed on the SEC separated fractions. The investigated species are the fully sulfated tetrasaccharide, hexasaccharide and octasaccharide. The effect of the charge was also investigated by measuring the $z = N$ and the $z = N + 1$ species. For these kinds of measurements normally the most iconic value is the so-called survival yield 50 (SY50), which gives the applied energy at the inflection point of the curve. Since we do not only look at the degradation of a species but also at the buildup, the resulting curve is not a sigmoid function but instead a gaussian like function. The turning point in which more species are destroyed than created is in this case more iconic and therefore used.

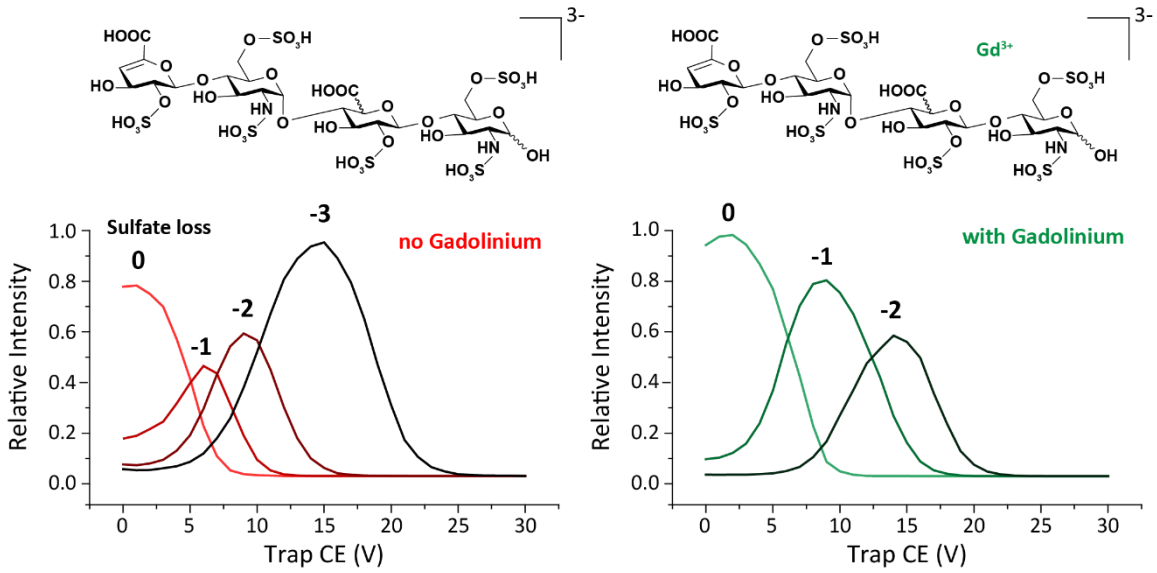

Figure 18: *Energy resolved measurement of the tetrasaccharide shows sulfate stability difference due to the gadolinium binding.*

As already showed the number of desulfations remains largely the same. Only for the tetrasaccharide one sulfate less is fragmenting off due to only two available carboxylic acid groups (see figure 18). Interestingly while the intensity of the desulfations seems to

rise from step to step in the deprotonated tetrasaccharide, the maximum intensity for the gadolinium species is dropping. This is seen for all sizes and charges (see appendix). The reason for this is likely the presence of several conformers and species in the gas phase with different degrees of contribution from the carboxylic acid group. Some gadolinium ions are only coordinating on one and some on two or three carboxylates. The desulfation steps occurred in a linear fashion according to the applied trap voltage. Out of the slope of the fitted line the relative stability of the sulfates can be read out (see table 1).

Table 1.: *Relative energy differences between desulfation of the different species. Deprotonated species are red marked, Gd species are green marked.*

N/z	2/2	2/3	3/3	3/4	4/4	4/5
ΔTpCE	5	3	3.3	2.6	2.54	2
	6	5	4	3.5	2.43	2.4

The species with a gadolinium attached to them showed an overall higher stability. The effect shrinks with higher saccharide number. The charge reduces the stability; all higher charged species show a lower value. The stability of the sulfate groups is also reduced by a higher degree of polymerization.

5.5 Fondaparinux Gadolinium Binding

The only commercially available completely synthesized GAG is Fondaparinux (see figure 19), which is used in the treatment of deep vein thrombosis.

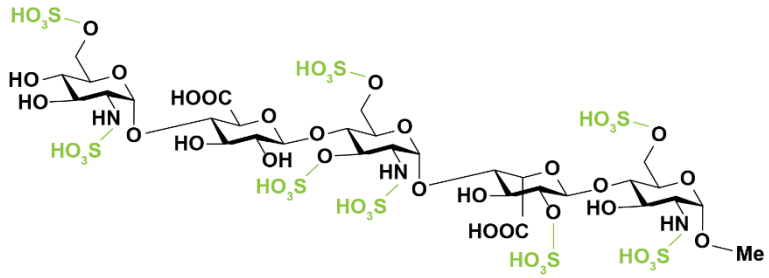

Figure 19: *Fondaparinux, the only available synthetic GAG.*

Fondaparinux consists of five monosaccharides from which three are glucosamines (GlcN), one glucuronic acid (GlcA) and one iduronic acid (IdoA). The reducing end is functionalized with a methyl group. To verify the measurements on enoxaparin the same measurements were performed on fondaparinux. Fondaparinux as completely protonated species is incredibly unstable in the gas phase. The main assignable observed species were the five-times desulfated triply charged ion and the four-times desulfated four-times

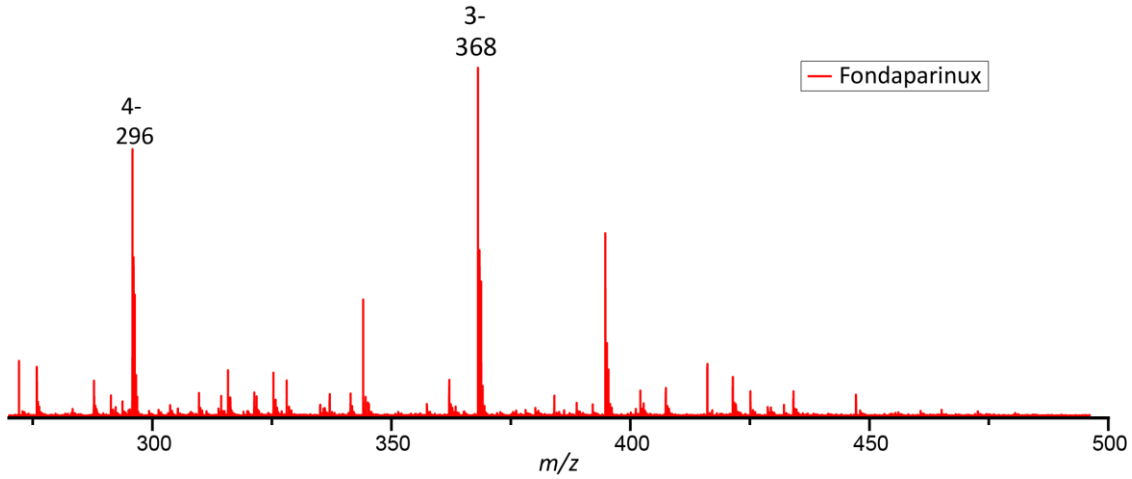

Figure 20: *Mass spectrum of the fondaparinux protomer only reveals the desulfated species.*

charged species (see figure 20). Nevertheless this is in good agreement with the enoxaparin; desulfation only happens till a point where charge equals the degree of sulfation (see figure 21). Same holds for the gadolinium species. For the quadropoly charged species only a maximum of three sulfates fragment off instead of the four anticipated. This is due to the limitation that fondaparinux only consist of two carboxylic groups, therefore gadolinium can only coordinate on two.

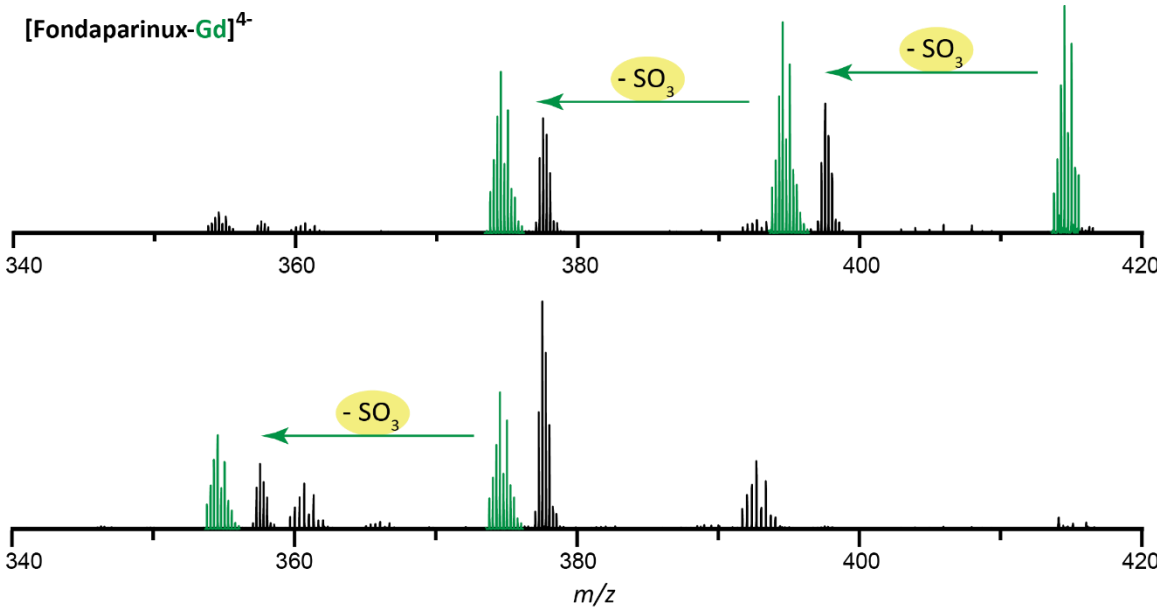

Figure 21: *Desulfation of the four-times charged fondaparinux-Gd species showed the same behavior as for enoxaparin-Gd. The large peaks next to the gadolinium species correspond to the sodium adducts.*

5.6 IR Spectroscopy on Fondaparinux

To confirm the data from the CID experiments gas-phase IR spectroscopy was performed on fondaparinux and its gadolinium species. A very prominent band of the GAGs is the *v*(C=O) stretching vibration. Depending on the state of the carboxylic acid this stretching vibrations are shifted. The vibration of the protonated carboxylic acid can be found between 1750 - 1850 cm^{-1} while the stretching vibration of the deprotonated carboxylic acid is located between 1600 – 1700 cm^{-1}. The IRMPD spectra of three protomers (Charge -3, -4, -5; *m/z* 501, 376, 250) were obtained (see figure 22). The scans were performed in a range between 1620 – 1850 cm^{-1}. The spectra showed similar results with a main absorption at around ~1760 cm^{-1}. The comparably broad peaks indicate a conformer rich sample but since the differences between them seem to be small, IMS is incapable to isolate them. The four-times charged species showed an additional absorption at 1710 cm^{-1}. This could be interpreted as a deprotonated carboxylic acid but could also result from this conformer richness. With higher charges on the fondaparinux the absorption peaks become narrower. This likely has two main reasons; the first being with the higher charge state the ion becomes more fragile and therefore the inherent redshift of IRMPD becomes less pronounced. The second reason is the reduced

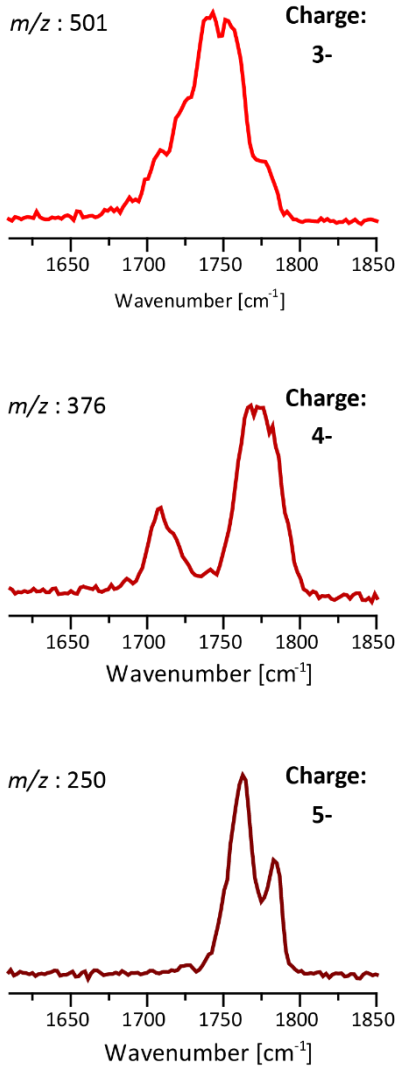

Figure 22: *IR spectra of the Fondaparinux protomers in the v(C=O) stretching vibration region.*

conformational freedom due to Coulomb repulsion of the additional charges in the molecule. For the fondaparinux-Gd species two charge states were measured (-4 and -5; *m/z* 414 and 331). The four-times charged species reveals in its ATD that two major kinds of conformers exist in the gas phase (see figure 23). Both conformer groups were ATD selected and measured separately in a photon energy range between 1000 - 1850 cm^{-1}. The two groups seem to differ only in the range between 1600 – 1850 cm^{-1}. The peaks in the range between 1000 – 1400 cm^{-1} can be mainly assigned to the sulfate vibrations as described in the literature.[45)]

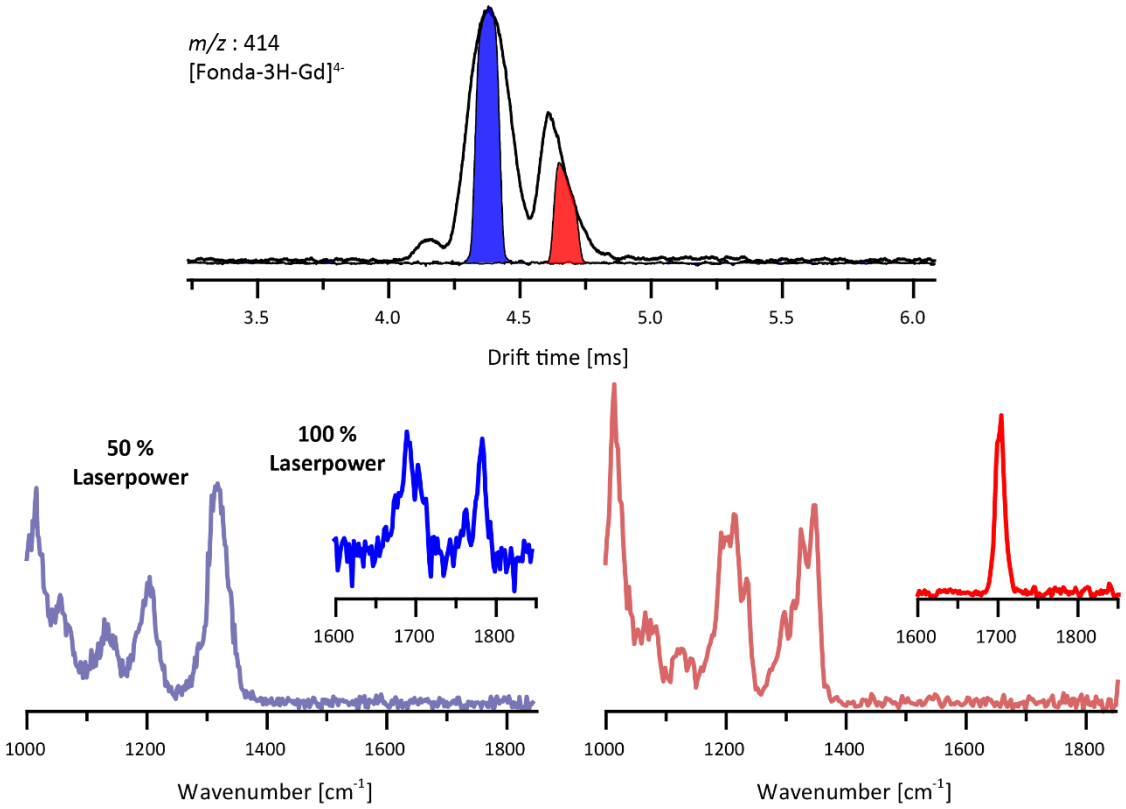

Figure 23: *IMS separation of the four-times charged fondaparinux-Gd species shows two groups of conformers in the ATD. IR spectra of the ATD selected species (marked in the corresponding colors) show different contributions of the carboxylic acid to the binding.*

At 1320 cm^{-1} the S=O stretching vibration of the free sulfate is found. Next to it lays at 1200 cm^{-1} the H-bonded S=O stretching vibration of the sulfates. At 1020 cm^{-1} the symmetric SO_3 vibration is found. This assigned absorptions likely overlap with the C-O stretching vibration which is often found between 1000 – 1150 cm^{-1} and the C-OH stretching vibration lays between 1150 – 1450 cm^{-1}. The more interesting part of the spectrum is seen between 1650 – 1850 cm^{-1}. Here a difference between the conformer groups is noticeable; the left, faster group shows two absorption peaks in this region. The peak at 1690 cm^{-1} corresponds to the carboxylate group and the peak at 1780 cm^{-1} to the protonated one. The right group in the ATD on the other hand only possesses one absorption peak at 1700 cm^{-1}, which matches the carboxylate vibration. The results are in good agreement with the energy resolved MS measurements on enoxaparin showing that not all carboxylic acids groups are bound to the gadolinium.

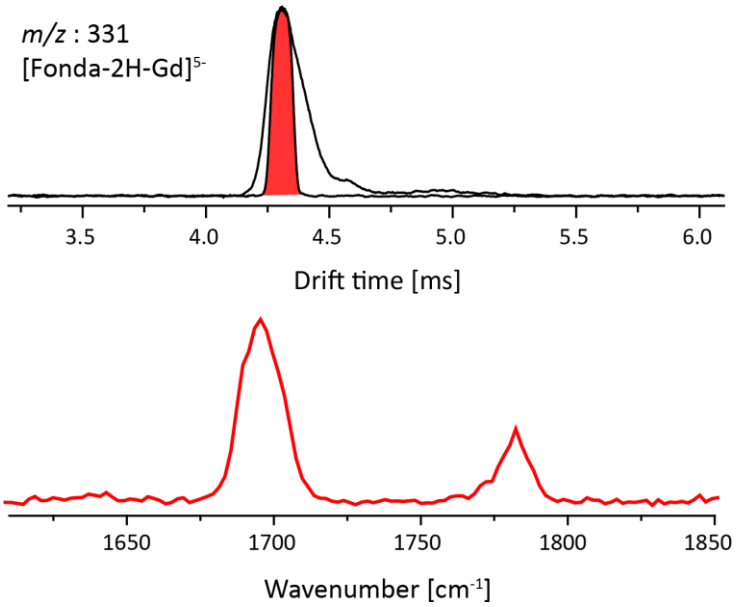

Figure 24: *IR spectrum between 1620 – 1850 cm^{-1} of the five-times negatively charged fondaparinux-Gadolinium complex. As for the four-times charged species both carboxylic and carboxylate absorption are visible.*

The absorption bands of the carboxylate show a heavy shift into higher wavenumbers (~70 cm-1), which often appears near 1630 cm-1. The five-times charged gadolinium species showed a very similar result (see figure 24). Absorptions at 1690 and 1780 cm-1 indicated the presence of both carboxylic acid and carboxylate. Only the ATD divert and shows one band. The intensity difference between the four-times and five-times charged species for the carboxylate could result due to a merging of the two ATD peaks in the four-times charged species into the one ATD peak in the five-times charged species. To confirm the assignment and to show that this binding is cation specific the four-times charged triple sodium adduct was measured (see figure 25). Similar to the four-times charged gadolinium species the sodium species showed two groups of conformers in the gas phase. Both peaks were ATD selected and measured in the energy region between 1620

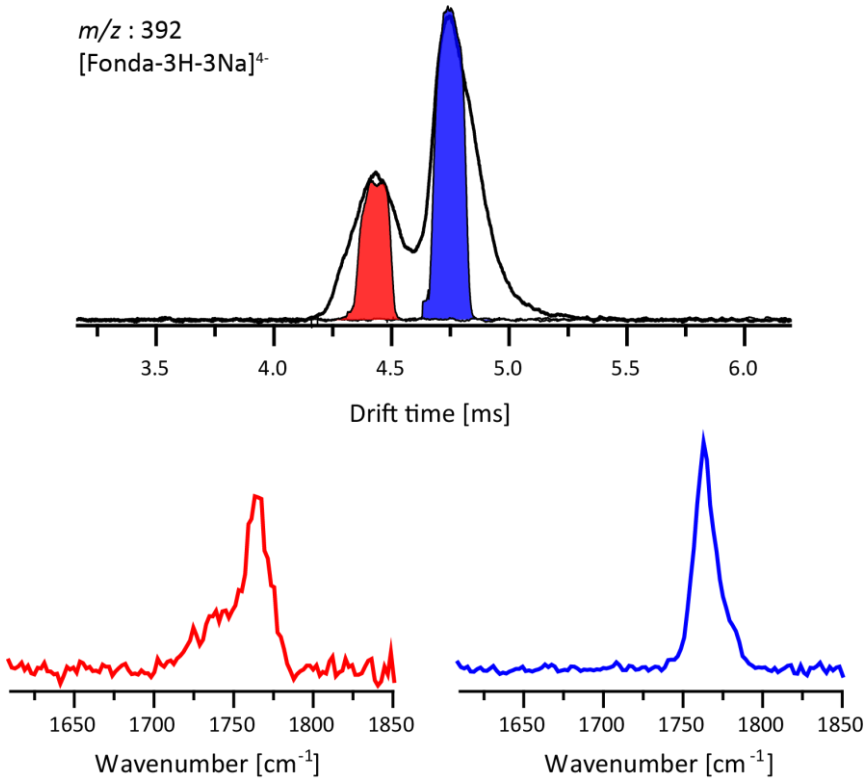

Figure 25: *The ATD of the four-times charged triple sodium adducts reveals two groups of conformers. For both no contribution to the binding on sodium of the carboxylic acid is seen.*

and 1850 cm^{-1}. As expected the sodium adducts showed for both cases only one absorption band at 1760 cm^{-1}. Interestingly the IR spectrum of the faster ATD peak (red) showed close resemblance to the absorption peak of the triply charged deprotonated species while the slower peak (blue) showed close resemblance to the five-times charged deprotonated species. It is to be expected that the higher charged species will more willingly form a linear structure in the gas phase due to Coulomb repulsion. This would cause not only an expansion of the molecule resulting in a higher drift time but also the afore mentioned reduced conformational freedom. Therefore the two observed ATD peaks are likely not resulting from different binding sites of the sodium on fondaparinux like it is the case for gadolinium but instead from the formation of a linear and globular form of the fondaparinux.

5.7 H/D Exchange on Fondaparinux

To address the deviant absorption peak of the four-times charged fondaparinux species more firmly H/D-exchange experiments were performed on it. The absorption at 1710 cm^{-1} is compared to the carboxylate vibration of the gadolinium species even more severely shifted to higher wavenumbers (~10 cm^{-1}) and could also just be a low field shifted C=O vibration of the carboxylic acid. To examine this thesis a H/D-exchange on the carboxylic acid could give definitive proof. The heavier isotope would lead to a red shift of the vibrations associated to the carboxylic acid while the carboxylate would be largely unaffected. Since the deuterium is not directly affected by the resonant C=O vibration but instead sits two bindings sites afar, the resulting shift should only be small but nevertheless present. Fondaparinux possesses 16 exchangeable protons; for the four-times charged species 12 remain. By exchanging all of them a mass shift of 3 *m/z* is expected and observed. The deuterium species was scanned in a range between 1500 – 1830 cm^{-1}. As before two peaks were seen: one at 1710 cm^{-1} and at 1770 cm^{-1} (see figure 26). Compared to the protonated species no significant change was observed. Neither of the peaks showed a shift and only a slight broadening was observed. A more resolving technique such as cryogenic IR spectroscopy could lead to a stronger conclusion.

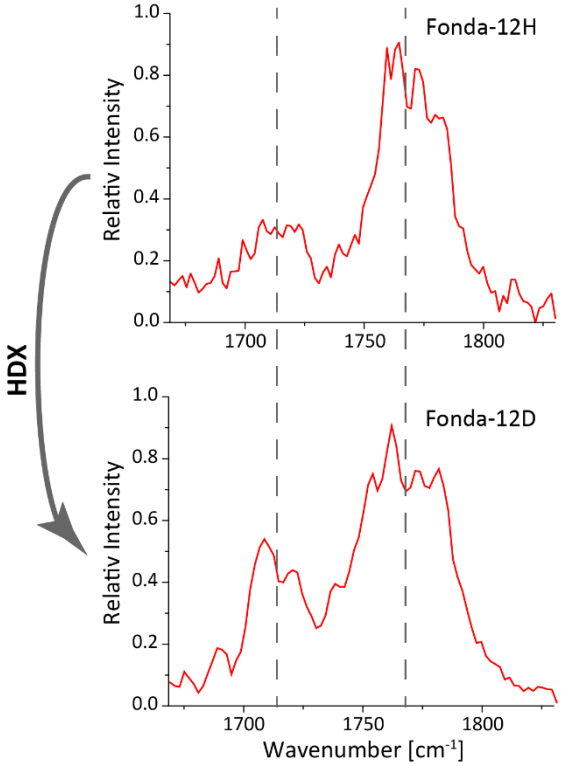

Figure 26: *IR spectra in the C=O stretching region shows no major difference between protonated and deuterated species.*

6. Summary

In this thesis the desulfation behavior of the low molecular weight heparin "enoxaparin" was investigated. It was shown by CID experiments that the charges introduced through the ESI process are sitting solely on the sulfate groups of the molecules. These charged sulfate groups will not fragment off by CID under neutral loss. This behavior was used to show that the lanthanide gadolinium is preferably binding to the carboxylic acid groups of enoxaparin. Additionally SEC separation was performed on enoxaparin and the obtained fractions were investigated by energy resolved MS. These measurements showed that the desulfation is enhanced by higher charges and/or a bigger size of the analyte. The coordination of gadolinium stabilizes the sulfates. This effect is larger for smaller molecules than for bigger ones.

The synthetic GAG fondaparinux was investigated by the same methods and has shown the same behavior. Additionally gas-phase IRMPD spectrometry was performed on it and its gadolinium complexes. Three different charge states of the protomer of fondaparinux were measured in the range between 1620 – 1850 cm^{-1} and all of them showed the iconic absorption band of the C=O stretching vibration of carboxylic acids. The measurement on the gadolinium fondaparinux species showed an additional absorption for the carboxylate at 1690 cm^{-1}, which confirms the data obtained by CID experiments. Measurements on the sodium fondaparinux species confirmed the distinctiveness of the gadolinium binding (see figure 27).

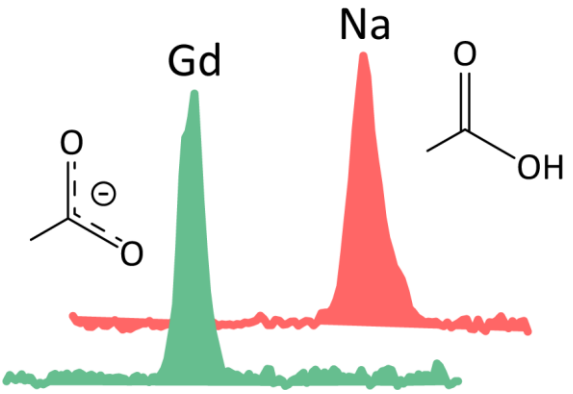

Figure 27: *Schematic overview of the measured IR spectroscopy data.*

7. Outlook

A main limiting factor of the work presented here is the sample acquisition. With more defined samples (specific sulfation sites and degree of sulfation, known monosaccharides) a more in-debt look into the binding of gadolinium could be obtained without major changes to the used methods. Therefore the next step in this project is the isolation and purification of GAGs from enoxaparin. SEC separation is only the first step; strong ion exchange chromatography has shown several times its great capability in the separation of GAGs.[46, 47] Also porous graphitic carbon chromatography is widely applied in glycan purification and could help in the preparation of GAG samples.[48] An HPLC system built up for this purpose is already standing at the Freie Universität Berlin and will be used to further elucidate the oddities of the gadolinium-GAG binding.

The MS data presented in this work was only used to get qualitative information out of the binding (not all carboxylic acid are involved in the binding). With the right normalization it may be possible to get quantitative information on the different binding site contributions. Additionally the method presented in this work could be used to effectively screen the binding site of all metals on GAGs not only gadolinium.

8. Experimental

8.1 Synapt-G2-S HDMS

Most MS and CID measurements were performed on a modified Synapt-G2-S HDMS (see figure 28).[49] The ions are introduced into the mass spectrometer through the ionization source (a n-ESI source) at atmospheric pressure. The ions now pass the step wave ion guide where neutral species and possible not fully evaporated droplets are being removed. Then they enter the quadrupole where a *m*/*z*-selection is possible. Now the ions enter the triwave region. The ions can be fragmented by CID in the trap and/or transfer cell. The IMS cell is located in between the fragmentation cells. In this work, a modified drift cell was used. The original TWIMS is replaced by a linear DTIMS, which is operated at 2.2 Torr helium pressure. After the triwave region the ions enter the dual stage reflectron time of flight (TOF) analyzer, where the mass separation occurs. Finally the mass separated ions hit the detector and a signal gets transmitted.

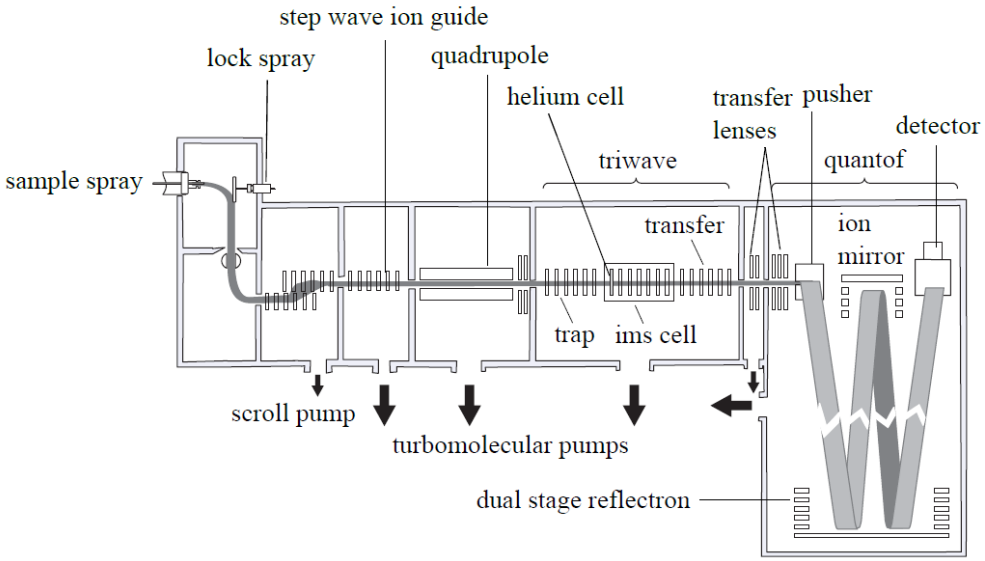

Figure 28: *Overview of the used Synapt-G2-S HDMS instrument.*

8.2 Ion Mobility Drift Tube Instrument (iMob)

The IR spectra were recorded on a home built drift tube ion mobility instrument (see figure 29), which is described in detail elsewhere.[50, 51] This instrument uses an n-ESI ionization source to generate ions, which are then collected at the entrance funnel and further pulsed into the drift tube ion mobility cell. The IMS cell is operated at 5 mbar Helium pressure and is using a weak electric field of 10-20 V/cm to pull the ions through it. After the IMS cell the ions are focused by an exit funnel and travel through ion guides into the high vacuum region containing two quadrupoles. The first quadrupole is used to isolate specific *m*/*z* ions from the ion package and the second functions as an ion guide or interaction region, which leads the ions either into the TOF mass analyzer or a detector plate to measure the observed arrival time distribution. A window at the end of the instrument allows it to introduce a light source in into the ion path. In combinations with a free electron laser (FEL), or a similar intense tunable light source, it is possible to induce photodissociation, which allows to record spectra through the principle of action spectroscopy.

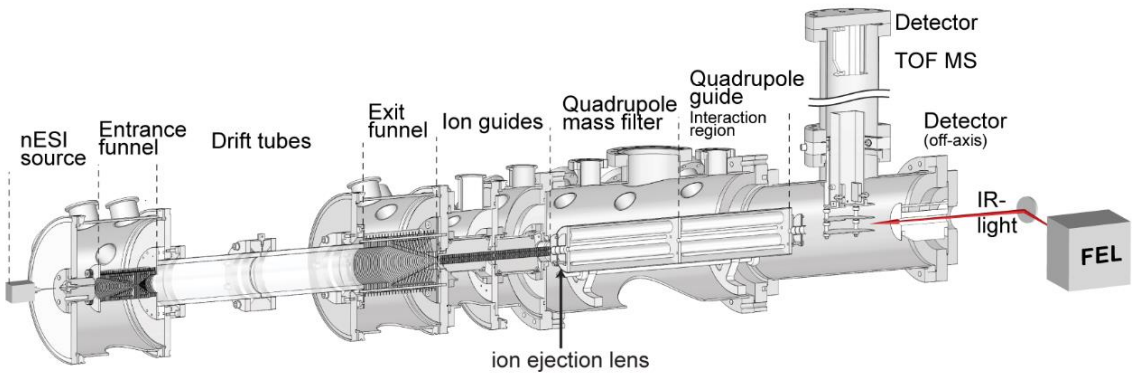

Figure 29: *Experimental setup of the used drift tube ion mobility instrument to acquire IRMPD spectra.*

8.3 Fritz Haber Institute Free Electron Laser

The general setup of a free electron laser (FEL) consists of an electron gun, a resonator including a built-in undulator and a beam dump. In the FHI-FEL[52] (see figure 30) the electron gun emits electrons, which are accelerated by two linear particle accelerators. The beam is then bent into the resonator, which consist of two highly reflective mirrors at each site. In between these mirrors an undulator is built in. The undulator consists of altering permanent magnets, which divert the electron beam perpendicular to the propagation direction. The resulting "wiggling" motion yields comparably weak synchrotron radiation. This weak spontaneous emission is increased by 10^6 - 10^8 magnitudes through the interaction of the light with previous electron packets inside the resonator (stimulated emission).[53] After passing the resonator the electron beam hits a beam dump and the light is redirected from the resonator through a small hole into the beam system, which is then diverted into the experiments.

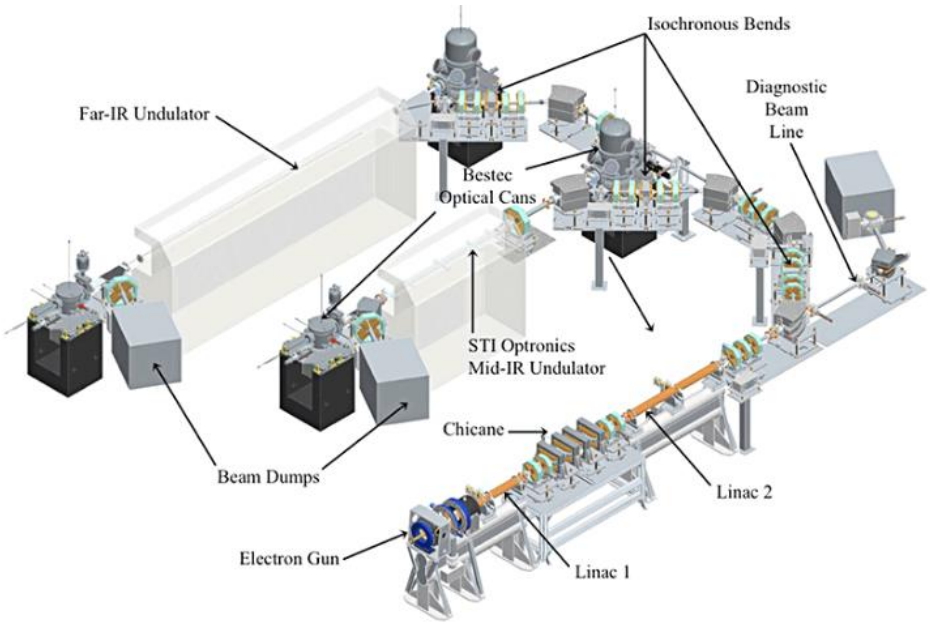

Figure 30: *Experimental setup of the Fritz-Haber-Institute (FHI) free electron laser (FEL).*

8.4 Mass Spectrometry on Enoxaparin and Fondaparinux

Solvents and Chemicals

Solvents for MS measurements were obtained from VWR Prolab and Sigma Aldrich. Fondaparinux was obtained from Sigma Aldrich as a pure component. Enoxaparin was also obtained from Sigma Aldrich but manufactured by European Pharmacopoeia. The gadolinium nitrate was obtained from Carl Roth.

Measurement Details

All measurements were performed with n-ESI with a 1:1 solvent mixture of Methanol and Water. The concentration of enoxaparin was 50 mg/L. The fondaparinux MS measurements concentration was 250 μM. Gadolinium concentration in the sample for the enoxaparin measurements was 120 μM and for the fondaparinux measurements 250 μM. The needle voltage on the Synapt was set to 0.8 – 1.0 kV. The settings were optimized to reduce unwanted desulfation while sustaining an intense ion count. Most important settings were the wave height in the trap cell (0.5 V) and the DC entrance voltage (1 V). Analysis of the data was performed with the Waters MassLynx software V4.1.

Energy Resolved Measurements

Energy resolved measurements were performed with the modified Synapt G2-S HMDS. The species to be examined was isolated in the quadrupole and the voltage in the trap cell of the triwave region was incrementally increased by one volt. The transfer cell was turned off. Every spectrum was recorded for half a minute (total 15.5 min) and an energy range from 0 to 30 V was covered. The intensity of the investigated species was noted for each spectrum and then normalized to the respective total ion count.

8.5 HPLC settings for SEC separation

HPLC system:	Thermo Fischer Dionex Ultimate 3000 Nano-LC
Column:	Phenomenex Yarra sec-x150 (1.8 µm, 300 x 4.6 mm)
Pressure:	210 Bar / 3045 psi
Flowrate:	200 µL/min
Mobile Phase:	50 mM NH_4AC without pH adjustment / MeOH (80:20) over 25 min
Sample volume:	2 µL
Sample:	Enoxaparin (solved in mobile phase) 50 µg/µL
Detection:	UV 232 nm

Solvents

Solvents for the HPLC separation were obtained from VWR Prolab and Sigma Aldrich. The deionised water for the HPLC separation was obtained from a Thermo Fischer water purification system.

Mass Spectrometry

Recorded mass spectra of the obtained fractions were measured on the modified Synapt G2-S HDMS instrument. Settings were optimized to reduce unwanted desulfation in the "Sensitive"-mode of the instrument. Analysis of the data was performed with the Waters MassLynx software V4.1.

8.6 IMS and IRMPD Measurements on Fondaparinux

All IRMPD measurements were performed on the home built drift tube instrument in collaboration with the doctorate student Maike Lettow from the Fritz Haber Institute.

Sample

The concentration of fondaparinux for the IRMPD measurement was 50 μM. Fondaparinux was dissolved in 1:1 water/methanol. For the gadolinium species an equivalent amount of gadolinium was added (50 μM/L).

IMS and MS

The drift tube ion mobility measurements were performed using helium as a drift gas. The pressure in the drift tube was hold at ~5 mbar. An electric field of 10 – 20 V/cm was held inside the drift tube. The needle voltage ranged from 0.8–1.1 kV.

FEL

The FEL was coupled to the DTIMS instrument. The FEL provided a laser power that ranged from 60–100 mJ/pulse with a pulse length of 10 μs. The scanning for the spectra was performed by steps of 2 cm^{-1}. 25-75 averages were used per recorded point.

H/D Exchange

The H/D exchange was performed by dissolving fondaparinux in deuterated water and methanol (1:1) and infusing the cone gas of the instrument with heavy water.

9. Literature

1) M. A. Kirchin, G. Pirovano, C. Venetianer and A. Spinazzi, *Journal of Magnetic Resonance Imaging*, **2001**, 14, *281*.
2) V. Aslanian, H. Lemaignen, P. Bunouf, M. G. Svaland, A. Borseth and B. Lundby, *Neuroradiology*, **1996**, 38, *537*.
3) T. Grobner, *Nephrology Dialysis Transplantation*, **2006**, 21, *1104*.
4) J. Jamboti, *Internal Medicine Journal*, **2007**, 37, *508*.
5) J. C. Weinreb and A. K. Abu-Alfa, *Journal of Magnetic Resonance Imaging*, **2009**, 30, *1236*.
6) N. R. PUTTAGUNTA, W. A. GIBBY and V. L. PUTTAGUNTA, *Investigative Radiology*, **1996**, 31, *619*.
7) S. LAURENT, L. VANDER ELST, F. COPOIX and R. N. MULLER, *Investigative Radiology*, **2001**, 36, *115*.
8) A. D. Sherry, P. Caravan and R. E. Lenkinski, *Journal of Magnetic Resonance Imaging*, **2009**, 30, *1240*.
9) V. H. Pomin and B. Mulloy, *Pharmaceuticals*, **2018**, 11, *27*.
10) M. Kopec, A. Imiela and H. Abramczyk, *Scientific Reports*, **2019**, 9, *166*.
11) M. Taupitz, N. Stolzenburg, M. Ebert, J. Schnorr, R. Hauptmann, H. Kratz, B. Hamm and S. Wagner, *Contrast Media & Molecular Imaging*, **2013**, 8, *108*.
12) A. Almond, *Cellular and Molecular Life Sciences*, **2007**, 64, *1591*.
13) J. L. Funderburgh, *Glycobiology*, **2000**, 10, *951*.
14) K. Sugahara, T. Mikami, T. Uyama, S. Mizuguchi, K. Nomura and H. Kitagawa, *Current Opinion in Structural Biology*, **2003**, 13, *612*.
15) C. J. Jones, S. Beni, J. F. K. Limtiaco, D. J. Langeslay and C. K. Larive, *Annual Review of Analytical Chemistry*, **2011**, 4, *439*.
16) M. J., *U.S. Patent* No., **1984**, 4,440,926.
17) U. R. Desai, H. M. Wang and R. J. Linhardt, *Biochemistry*, **1993**, 32, *8140*.
18) K. A. Jandik, K. Gu and R. J. Linhardt, *Glycobiology*, **1994**, 4, *289*.
19) R. D. Hull and G. Townshend, *Thromb Haemost*, **2013**, 110, *14*.
20) E. Gray, B. Mulloy and T. W. Barrowcliffe, *Thromb Haemost*, **2008**, 99, *807*.
21) J. Hofmann, H. S. Hahm, P. H. Seeberger and K. Pagel, *Nature*, **2015**, 526, *241*.
22) A. Horne and P. Gettins, *Carbohydrate Research*, **1992**, 225, *43*.
23) J. J. Wolff, L. Chi, R. J. Linhardt and I. J. Amster, *Analytical Chemistry*, **2007**, 79, *2015*.

24) I. Agyekum, C. Zong, G.-J. Boons and I. J. Amster, *Journal of The American Society for Mass Spectrometry*, **2017**, 28, *1741*.

25) M. R. Schenauer, J. K. Meissen, Y. Seo, J. B. Ames and J. A. Leary, *Analytical Chemistry*, **2009**, 81, *10179*.

26) F. E. Leach, N. M. Riley, M. S. Westphall, J. J. Coon and I. J. Amster, *Journal of The American Society for Mass Spectrometry*, **2017**, 28, *1844*.

27) R. Huang, J. Liu and J. S. Sharp, *Analytical Chemistry*, **2013**, 85, *5787*.

28) F. Chevalier, J. Angulo, R. Lucas, Pedro M. Nieto and M. Martín-Lomas, *European Journal of Organic Chemistry*, **2002**, 2002, *2367*.

29) K. Mazák, C. N. Beecher, M. Kraszni and C. K. Larive, *Carbohydrate Research*, **2014**, 384, *13*.

30) Y. Seo, M. R. Schenauer and J. A. Leary, *International Journal of Mass Spectrometry*, **2011**, 303, *191*.

31) M. Remko, P. T. Van Duijnen and R. Broer, *RSC Advances*, **2013**, 3, *9843*.

32) M. Remko, R. Broer, A. Remková and P. T. Van Duijnen, *Chemical Physics Letters*, **2015**, 621, *12*.

33) D. R. Ferro, A. Provasoli, M. Ragazzi, B. Casu, G. Torri, V. Bossennec, B. Perly, P. Sinaÿ, M. Petitou and J. Choay, *Carbohydrate Research*, **1990**, 195, *157*.

34) D. L. Rabenstein, J. M. Robert and J. Peng, *Carbohydrate Research*, **1995**, 278, *239*.

35) in *Practical High-Performance Liquid Chromatography*, DOI: 10.1002/0470032677.ch15, pp. 207.

36) L. Konermann, E. Ahadi, A. D. Rodriguez and S. Vahidi, *Analytical Chemistry*, **2013**, 85, *2*.

37) J. Fenn, M. Mann, C. Meng, S. Wong and C. Whitehouse, *Science*, **1989**, 246, *64*.

38) M. Karas, U. Bahr and T. Dülcks, Fresenius' *Journal of Analytical Chemistry*, **2000**, 366, *669*.

39) V. Gabelica and E. Marklund, *Current Opinion in Chemical Biology*, **2018**, 42, *51*.

40) K. Giles, *International Journal for Ion Mobility Spectrometry*, **2013**, 16, *1*.

41) L. Sleno and D. A. Volmer, *Journal of Mass Spectrometry*, **2004**, 39, *1091*.

42) J. Oomens, B. G. Sartakov, G. Meijer and G. von Helden, *International Journal of Mass Spectrometry*, **2006**, 254, *1*.

43) B. Lucas, G. Grégoire, J. Lemaire, P. Maître, F. Glotin, J. P. Schermann and C. Desfrançois, *International Journal of Mass Spectrometry*, **2005**, 243, *105*.

44) W. Chai, J. Luo, C. K. Lim and A. M. Lawson, *Analytical Chemistry*, **1998**, 70, *2060*.

45) B. Schindler, L. Barnes, C. J. Gray, S. Chambert, S. L. Flitsch, J. Oomens, R. Daniel, A. R. Allouche and I. Compagnon, *The Journal of Physical Chemistry A*, **2017**, 121, *2114*.

46) R. L. Miller, S. E. Guimond, M. Shivkumar, J. Blocksidge, J. A. Austin, J. A. Leary and J. E. Turnbull, *Analytical Chemistry*, **2016**, 88, *11542*.

47) J. M. Fasciano and N. D. Danielson, *Journal of Separation Science*, **2016**, 39, *1118*.

48) K. Stavenhagen, D. Kolarich and M. Wuhrer, *Chromatographia*, **2015**, 78, *307*.

49) *https://www.waters.com/waters/en_US/SYNAPT-G2-Si-High-Definition-Mass-Spectrometry/*, **2019**.

50) S. Warnke, G. von Helden and K. Pagel, *PROTEOMICS*, **2015**, 15, *2804*.

51) P. R. Kemper, N. F. Dupuis and M. T. Bowers, *International Journal of Mass Spectrometry*, **2009**, 287, *46*.

52) *http://fel.fhi-berlin.mpg.de/*, **2019**.

53) J. Ullrich, A. Rudenko and R. Moshammer, *Annual Review of Physical Chemistry*, **2012**, 63, *635*.

10. Appendix

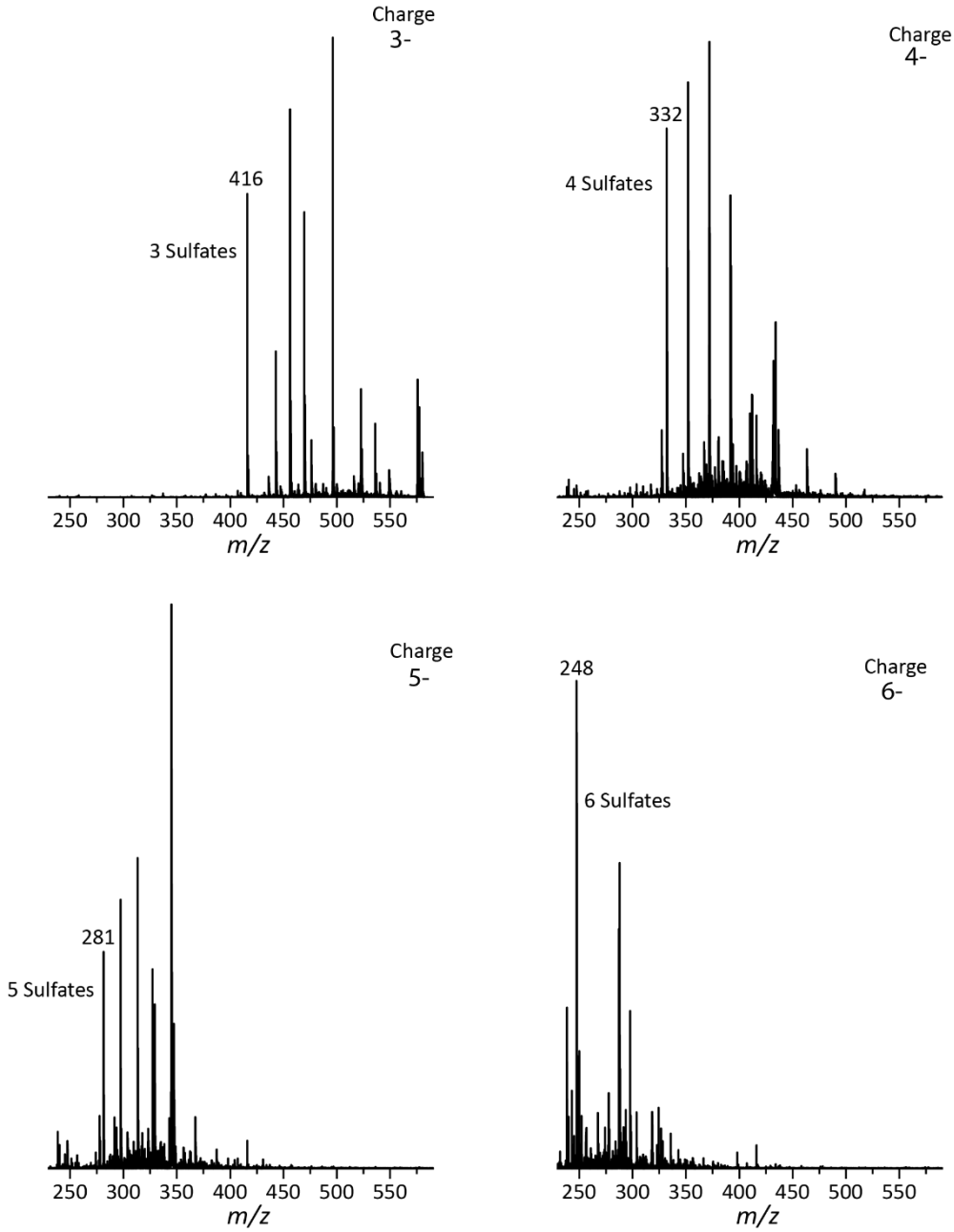

Figure 31: *Desulfation of different charge states shows that the minimal sulfate count equals the charge.*

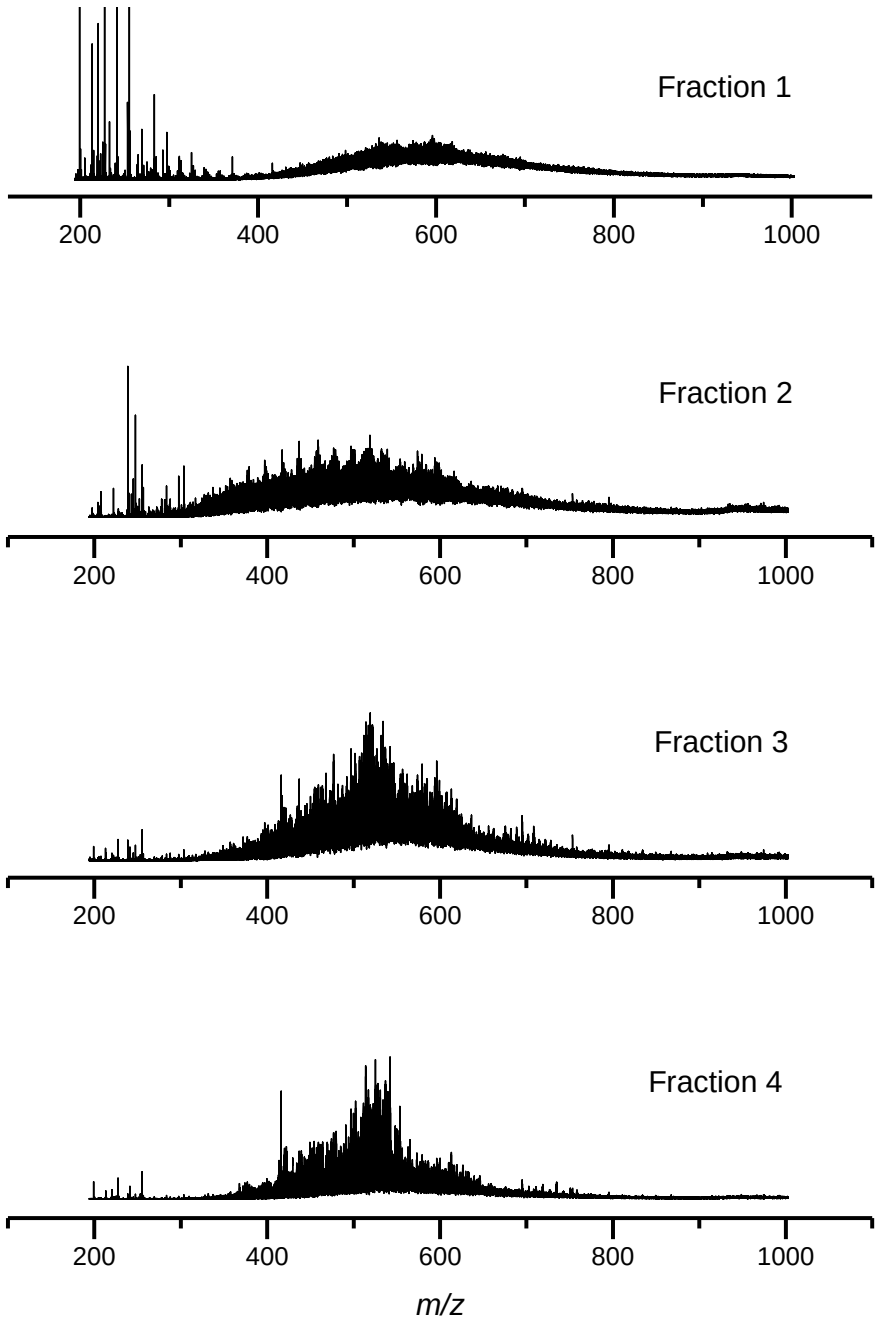

Figure 32: *MS spectra obtained from the SEC separated fractions 1-4.*

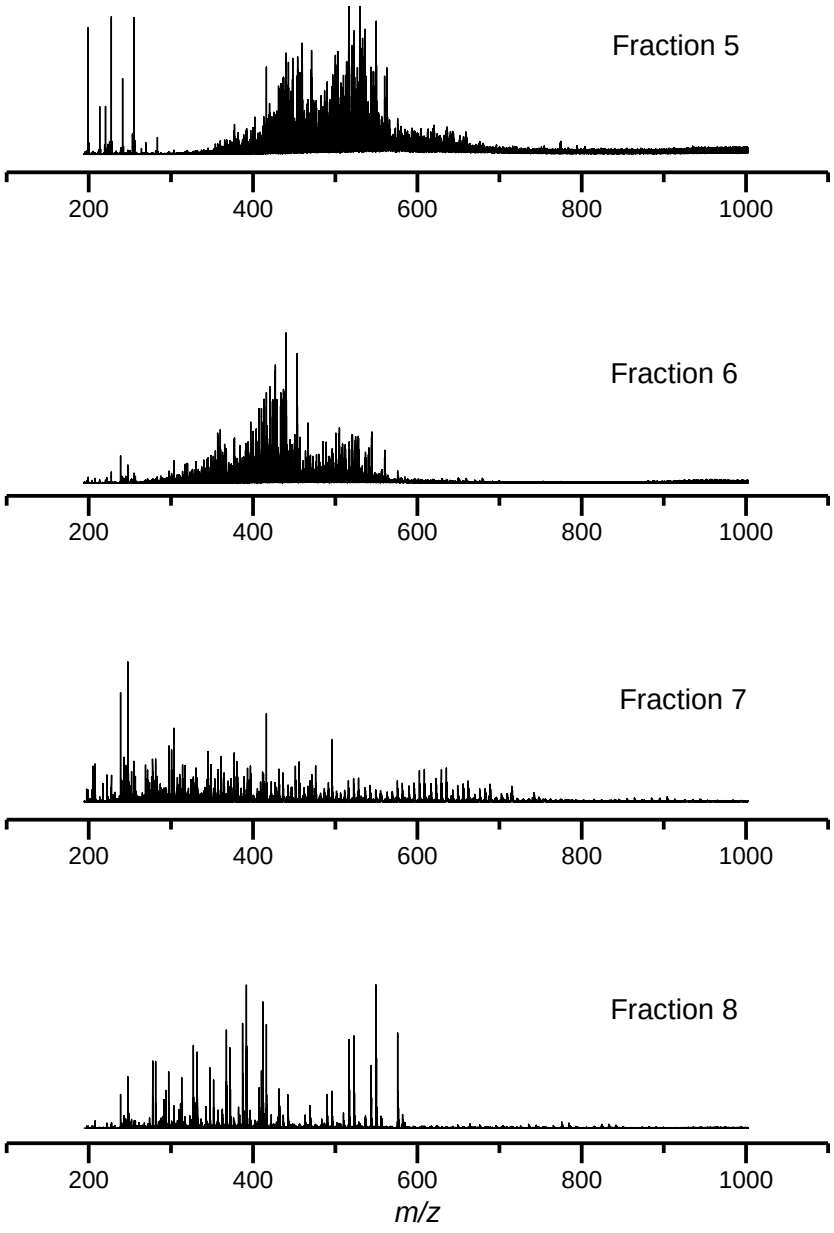

Figure 33: *MS spectra obtained from the SEC separated fractions 5-8.*

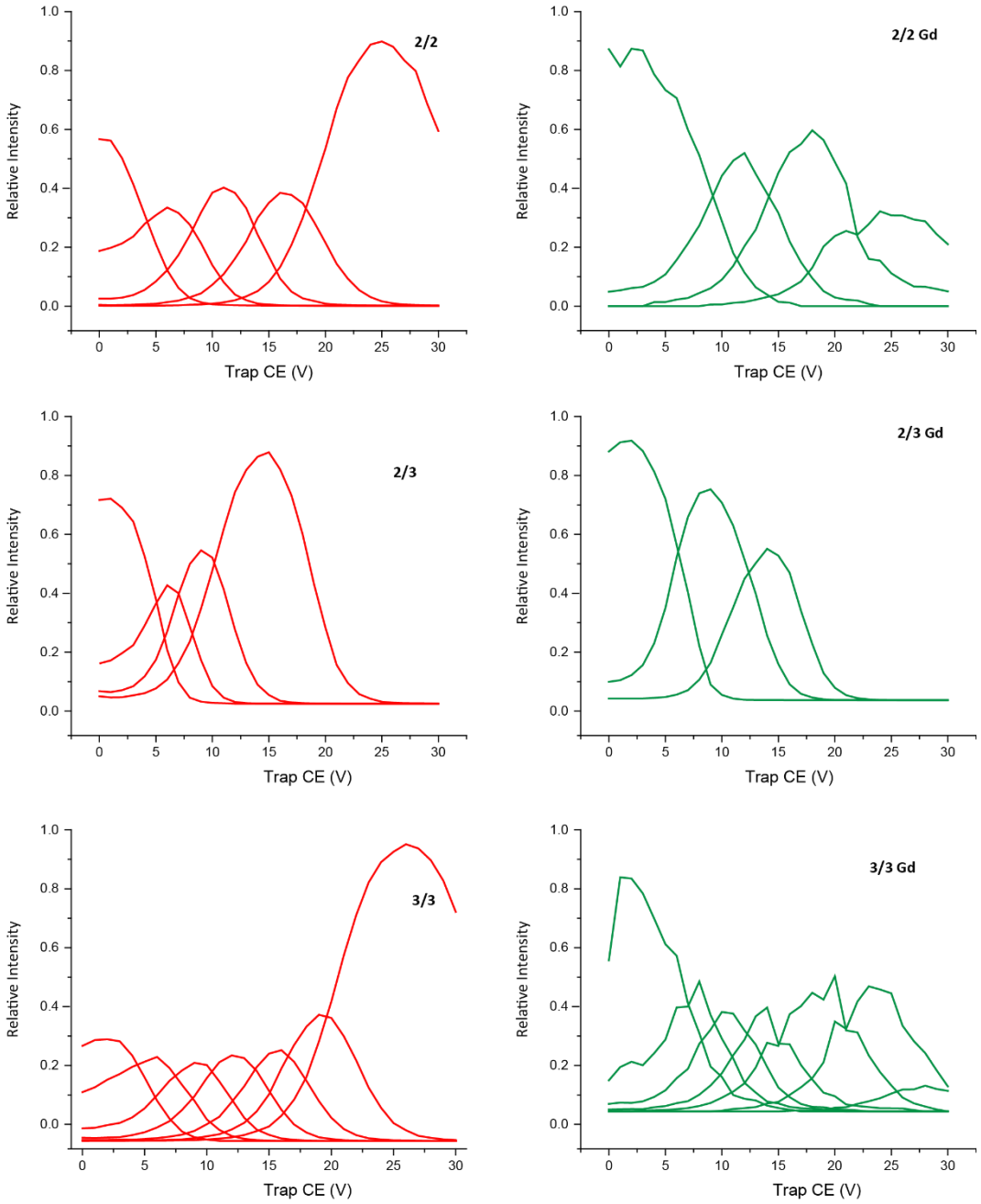

Figure 34: *Energy resolved mass spectra of the SEC separated fractions. Red without gadolinium; green with gadolinium.*

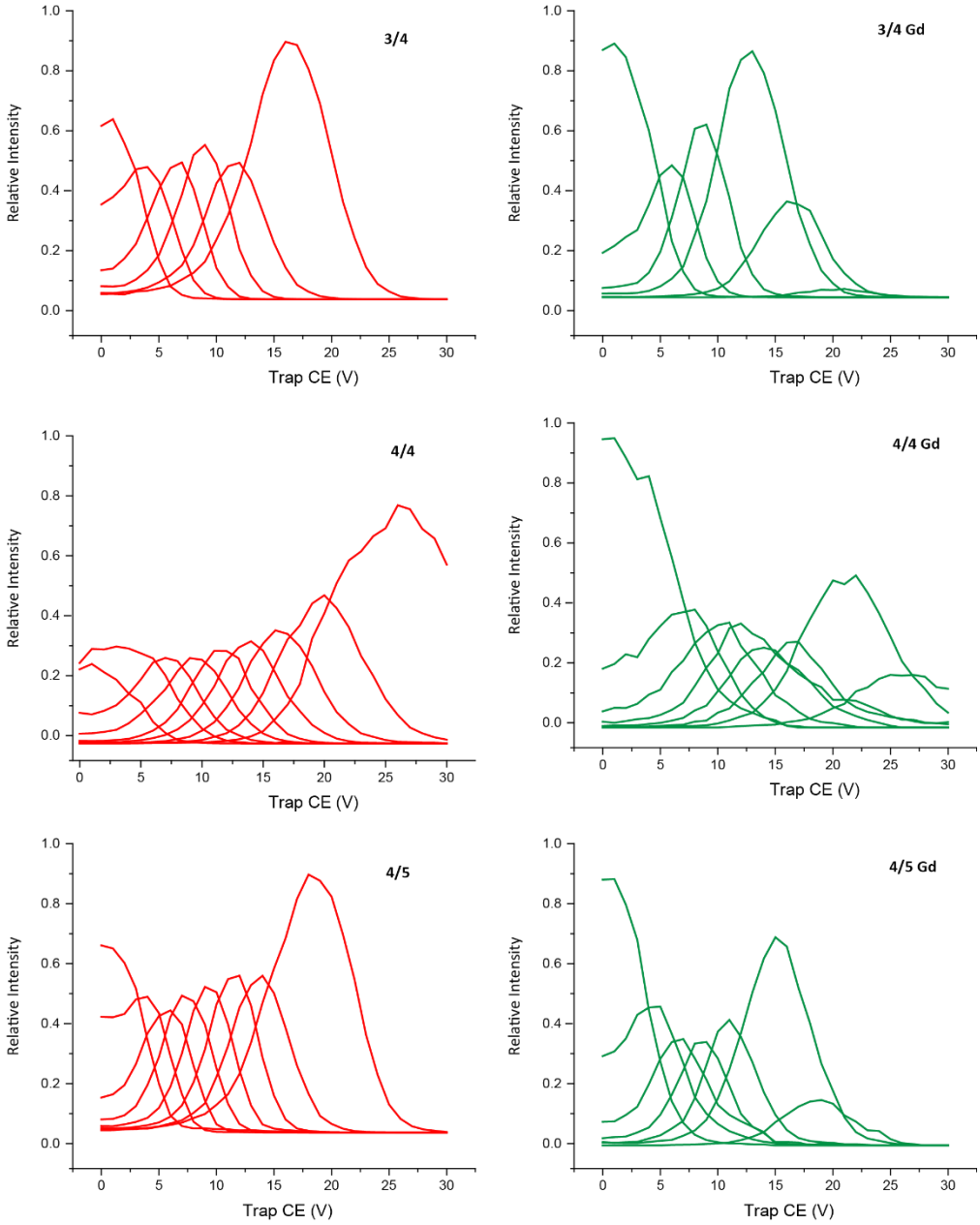

Figure 35: *Energy resolved mass spectra of the SEC separated fractions. Red without gadolinium; green with gadolinium.*

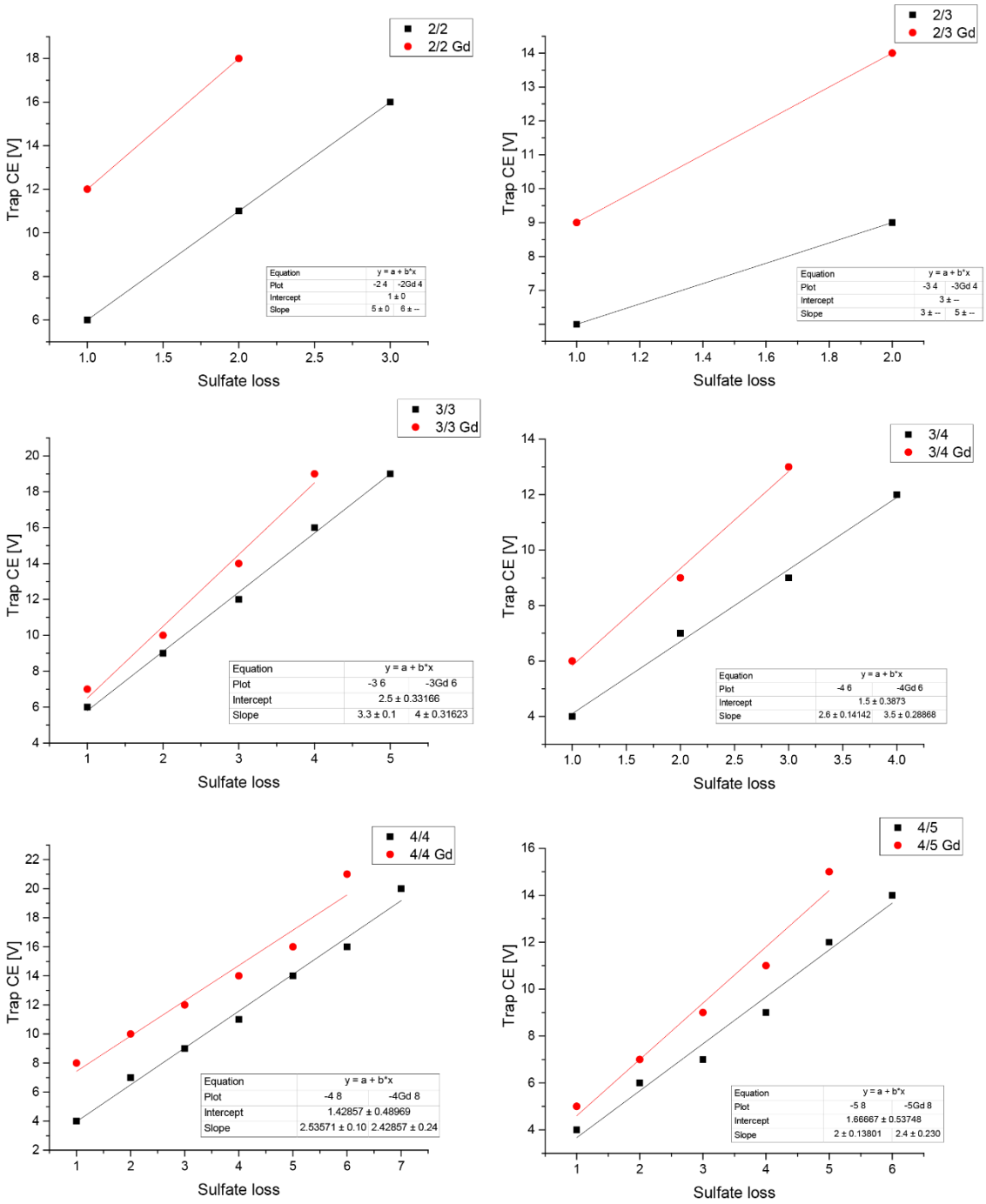

Figure 36: *Fitting curves of the desulfations against the trap energy.*

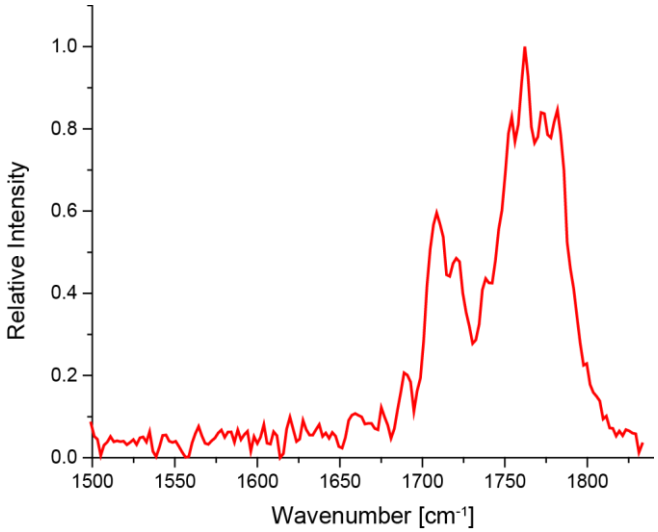

Figure 37: *Full recorded IRMPD spectrum of the four-times negatively charged fully deuterated fondaparinux.*